Three-wave scattering in magnetized plasmas: From cold fluid to quantized Lagrangian

Yuan Shi,[1,2,*] Hong Qin,[1,2,3] and Nathaniel J. Fisch[1,2]

[1]*Department of Astrophysical Sciences, Princeton University, Princeton, New Jersey 08544, USA*

[2]*Princeton Plasma Physics Laboratory, Princeton University, Princeton, New Jersey 08543, USA*

[3]*School of Nuclear Science and Technology, University of Science and Technology of China, Hefei, Anhui 230026, China*

(Received 26 May 2017; published 14 August 2017)

Large amplitude waves in magnetized plasmas, generated either by external pumps or internal instabilities, can scatter via three-wave interactions. While three-wave scattering is well known in collimated geometry, what happens when waves propagate at angles with one another in magnetized plasmas remains largely unknown, mainly due to the analytical difficulty of this problem. In this paper, we overcome this analytical difficulty and find a convenient formula for three-wave coupling coefficient in cold, uniform, magnetized, and collisionless plasmas in the most general geometry. This is achieved by systematically solving the fluid-Maxwell model to second order using a multiscale perturbative expansion. The general formula for the coupling coefficient becomes transparent when we reformulate it as the scattering matrix element of a quantized Lagrangian. Using the quantized Lagrangian, it is possible to bypass the perturbative solution and directly obtain the nonlinear coupling coefficient from the linear response of the plasma. To illustrate how to evaluate the cold coupling coefficient, we give a set of examples where the participating waves are either quasitransverse or quasilongitudinal. In these examples, we determine the angular dependence of three-wave scattering, and demonstrate that backscattering is not necessarily the strongest scattering channel in magnetized plasmas, in contrast to what happens in unmagnetized plasmas. Our approach gives a more complete picture, beyond the simple collimated geometry, of how injected waves can decay in magnetic confinement devices, as well as how lasers can be scattered in magnetized plasma targets.

DOI: 10.1103/PhysRevE.96.023204

I. INTRODUCTION

Coherent three-wave scattering is perhaps the simplest and the most common type of nonlinear interaction in plasmas. It happens, for example, in magnetic confinement devices, where waves injected by antenna arrays decay to other waves [1,2]. In the case where the wave is injected to drive current in a tokamak [3,4], there is a possibility that the lower hybrid current drive is affected by unwanted decays near the tokamak periphery [5,6]. Even more importantly, three-wave scattering also happens, for example, in laser implosion experiments [7], where high intensity lasers interact with plasmas. During magnetized implosions, where the magnetic field is imposed to enhance particle confinement [8–10], multiple laser beams may scatter and reflect one another via magnetic resonances. In fact, the magnetic resonances can be utilized to mediate energy transfer between laser beams to achieve pulse amplification [11], where three-wave scattering plays an essential role.

Despite its importance, coherent three-wave scattering, well studied in unmagnetized plasma [12,13], remains poorly understood when plasmas become magnetized. This situation is mostly due to the analytical difficulty when external magnetic field is present. Such difficulty deserves to be overcome in the midst of recent developments in strong magnetic field technologies [14–16]. Using these technologies, magnetic fields on the order of mega-Gauss or even giga-Gauss can be produced. Such strong magnetic field makes electron gyrofrequency comparable to the plasma frequency in laser implosion experiments, in which the anisotropy introduced by the magnetic field can play a prominent role. Since multiple laser beams usually propagate at angles to one another and with the magnetic field during laser-driven implosions, understanding the angular dependence of three-wave scattering in magnetized plasma becomes indispensable for making a knowledgeable choice of the experimental setups to optimize laser-plasma coupling.

By far, most theoretical work on laser scattering in magnetized plasmas is focused on the simple collimated geometry. In this simple geometry, three kinds of theories have been developed. The first kind is coupled mode theory, which searches for normal modes of the nonlinear equations [17,18]. Although normal modes satisfy formally simple equations, the complexity of the nonlinear problem is hidden inside obscure coupling coefficients, from which little physical meaning has been extracted. The second kind is nonlinear current theory, which describes three-wave parametric interaction by adding a nonlinear source term into the Maxwell's equations. Using fluid models for nonlinear sources, parametric growth rates have been obtained for extraordinary wave pump [19–21], lower-hybrid wave pump [22], as well as the right- and left-circularly polarized wave pumps [23]. To capture thermal effects, a simple treatment retains only thermal corrections to the dielectric tensor [24]. A more complete treatment also includes thermal corrections to the coupling tensor [25,26]. However, beyond the simple collimated geometry, such treatment becomes so cumbersome that decades of efforts have been spent on just simplifying the expressions [27–29], with very little extractable physical results [30,31]. Aside from the coupled mode theory and the nonlinear current theory, the third kind of theory uses Lagrangian formulation. In this more systematic approach, the interaction Lagrangian is obtained either from the Low's Lagrangian [32,33], or the oscillation-center Lagrangian [34] by expanding plasma response to the third order. Even with such transparent formalism, three-wave interactions in magnetized plasma,

*yshi@pppl.gov

where the waves are not collimated, remains to be analyzed systematically, in generality, and in detail.

In this paper, we overcome the analytical difficulty in fluid theory and obtain angular dependence of three-wave scattering in collisionless, cold, uniform, magnetized plasmas in the most general geometry. This is achieved by systematically solving the fluid-Maxwell system to second order in the perturbation series, where secular terms are removed using a multiscale expansion. Using this technique, we manage to obtain an expression for the coupling coefficient that is not only explicit, but also convenient, from which illuminating physical results can be extracted. Moreover, we show that the formula for the coupling coefficient naturally arises as the scattering matrix (S matrix) element of a quantized Lagrangian. This refreshing perspective, emerging from detailed cold fluid calculations, offers a high-level methodology, through which three-wave coupling can be easily computed. The cold fluid results are applicable when the wavelengths of participating waves are much longer than both the Debye length and the typical gyroradius. Within the applicable range of the fluid model, our nonrelativistic perturbative treatment is valid when the amplitudes of waves are not too large, so that the linear eigenmode structures are preserved, and spectrum broadening is limited. Our cold fluid results are useful for verification of numerical codes, as well as development of reduced models.

This paper is organized as follows. In Sec. II, we solve the fluid-Maxwell system to second order using a multiscale expansion. In Sec. III, we simplify the general equation in the simple case where there are only three linear waves participating in the interaction. In Sec. IV, we distill the classical theory into a quantized Lagrangian, where the formula for three-wave coupling becomes transparent. In Sec. V, we illustrate the general cold fluid results using a set of examples. Conclusion and discussion are given in Sec. VI, and supplementary information is provided in the Appendixes.

II. PERTURBATIVE SOLUTION OF FLUID-MAXWELL SYSTEM

In the fluid regime, where both the Debye length and the typical gyroradius are much smaller than the shortest wavelength, charged particles in the plasma respond collectively to perturbations. In this regime, the plasma system is well described by the fluid-Maxwell equations

$$\partial_t n_s = -\nabla \cdot (n_s \mathbf{v}_s), \tag{1}$$

$$\partial_t \mathbf{v}_s = -\mathbf{v}_s \cdot \nabla \mathbf{v}_s + \frac{e_s}{m_s}(\mathbf{E} + \mathbf{v}_s \times \mathbf{B}), \tag{2}$$

$$\partial_t \mathbf{B} = -\nabla \times \mathbf{E}, \tag{3}$$

$$\partial_t \mathbf{E} = c^2 \nabla \times \mathbf{B} - \frac{1}{\epsilon_0} \sum_s e_s n_s \mathbf{v}_s. \tag{4}$$

The continuity equation [Eq. (1)] describes the conservation of particles of species s, whose density is n_s and average velocity is $\mathbf{v}_s$. The momentum equation [Eq. (2)] governs how the velocity field $\mathbf{v}_s$ change due to both the advection and the Lorentz force, where e_s and m_s are the charge and mass of individual particles of species s. Finally, the magnetic field $\mathbf{B}$ evolves according to the Faraday's law [Eq. (3)], and the electric field $\mathbf{E}$ evolves according to the Maxwell-Ampère's law [Eq. (4)], where the current density is contributed by all charged species in the system.

The fluid-Maxwell equations [Eqs. (1)–(4)] are a system of nonlinear hyperbolic partial differential equations. Such a system of equations are in general difficult to solve. Nevertheless, when fluctuation near equilibrium is small, nonlinearities may be regarded as perturbations, and the equations may be solved perturbatively. To see when nonlinearities may be regarded as perturbations, we can normalize equations such that all quantities become dimensionless numbers. For example, we may normalize time to the plasma frequency ω_p and distance to the skin depth c/ω_p. We may further normalize mass to electron mass m_e, charge to elementary charge e, density to unperturbed density n_{s0}, and velocity to the speed of light c. Finally, we can normalize electric field to $m_e c\omega_p/e$ and normalize magnetic field to $m_e\omega_p/e$. With the above normalizations, the fluid-Maxwell equation can be written in dimensionless form. In this form, nonlinearities are products of small numbers and are therefore even smaller, provided that the perturbations are small.

In the absence of nonlinearities, the general solution to the fluid-Maxwell system is a spectrum of linear waves with constant amplitudes. Now imagine we can ramp up nonlinearities adiabatically, then waves will start to scatter one another. Due to weak scattering, amplitudes of waves will evolve slowly in space and time. This physical picture may be translated into a formal mathematical procedure. Formally, to solve the fluid-Maxwell equations peturbatively, it is helpful to keep track of terms by inserting an auxiliary small parameter $\lambda \ll 1$ in the perturbation series, and let the adiabatic parameter $\lambda \to 1$ in the end, mimicking the adiabatic ramping up of nonlinearities. The electric field, magnetic field, density, and velocity can be expanded using asymptotic series

$$\mathbf{E} = \mathbf{E}_0 + \lambda \mathbf{E}_1 + \lambda^2 \mathbf{E}_2 + \cdots, \tag{5}$$

$$\mathbf{B} = \mathbf{B}_0 + \lambda \mathbf{B}_1 + \lambda^2 \mathbf{B}_2 + \cdots, \tag{6}$$

$$n_s = n_{s0} + \lambda n_{s1} + \lambda^2 n_{s2} + \cdots, \tag{7}$$

$$\mathbf{v}_s = \mathbf{v}_{s0} + \lambda \mathbf{v}_{s1} + \lambda^2 \mathbf{v}_{s2} + \cdots, \tag{8}$$

where a self-consistent equilibrium is given by $\mathbf{E}_0 = \mathbf{0}$ and $\mathbf{v}_{s0} = \mathbf{0}$, while the background magnetic field $\mathbf{B}_0$ and density n_{s0} are some constants. It is well known that if we only expand field amplitudes, the naive asymptotic solution will contain secular terms for nonlinear problems. To remove the secular terms, we also need to do a multiscale expansion [35] in both space and time

$$x^i = x^i_{(0)} + \frac{1}{\lambda} x^i_{(1)} + \frac{1}{\lambda^2} x^i_{(2)} + \cdots, \tag{9}$$

$$t = t_{(0)} + \frac{1}{\lambda} t_{(1)} + \frac{1}{\lambda^2} t_{(2)} + \cdots, \tag{10}$$

where x^i is the ith component of vector $\mathbf{x}$. In the above expansion, $x^i_{(0)}$ is the shortest spatial scale. In comparison, one unit of $x^i_{(1)}$ is $1/\lambda$ times longer that one unit of $x^i_{(0)}$, and so on. Similarly, $t_{(0)}$ is the fastest time scale, and one unit of $t_{(n)}$ is

$1/\lambda^n$ times longer that one unit of $t_{(0)}$. In the above multiscale expansion, different spatial and temporal scales are regarded as independent

$$\partial_i^{(a)} x^j_{(b)} = \delta_i^j \delta^{(a)}_{(b)}, \tag{11}$$

$$\partial_t^{(a)} t_{(b)} = \delta^{(a)}_{(b)}, \tag{12}$$

and by chain rule, the total spatial and temporal derivatives are

$$\partial_i = \partial_i^{(0)} + \lambda \partial_i^{(1)} + \lambda^2 \partial_i^{(2)} + \cdots, \tag{13}$$

$$\partial_t = \partial_{t(0)} + \lambda \partial_{t(1)} + \lambda^2 \partial_{t(2)} + \cdots. \tag{14}$$

Using the multiscale expansion (11) and (12), together with expansion in field amplitudes (5)–(8), secular terms can be removed and the perturbative solution is well behaved. In Appendix A, we demonstrate how the multiscale expansion can be successively applied to a hyperbolic system of ordinary differential equations.

A. First order equations

Although the first order equations and their solutions are well known [36], here let us briefly review some important results, in order to introduce some notations that will be used in the next subsection. To obtain first order equations, we expand fields, space, and time in fluid-Maxwell equations, and collect all the $O(\lambda)$ terms

$$\partial_{t(0)} \mathbf{B}_1 = -\boldsymbol{\nabla}_{(0)} \times \mathbf{E}_1, \tag{15}$$

$$\partial_{t(0)} \mathbf{v}_{s1} = \frac{e_s}{m_s}(\mathbf{E}_1 + \mathbf{v}_{s1} \times \mathbf{B}_0), \tag{16}$$

$$\partial_{t(0)} n_{s1} = -n_{s0} \boldsymbol{\nabla}_{(0)} \cdot \mathbf{v}_{s1}, \tag{17}$$

$$\Box^{(0)}_{ij} E_1^j = -\frac{1}{\epsilon_0} \sum_s e_s n_{s0} \partial_{t(0)} v^i_{s1}. \tag{18}$$

Here, we have written the equations in the order that we are going to use them. The electric field equation (18) is obtained by substituting the Faraday's law (3) into the Maxwell-Ampère's equation (4), and then making the multiscale expansion. This procedure introduces the zeroth order differential operator

$$\Box^{(0)}_{ij} := \big(\partial^2_{t(0)} - c^2 \nabla^2_{(0)}\big)\delta_{ij} + c^2 \partial_i^{(0)} \partial_j^{(0)}. \tag{19}$$

This operator is the d'Alembert wave operator projected in the transverse direction.

Since the first order equations are linear, the general solution is a superposition of plane waves. Let us write the electric field in the form

$$\mathbf{E}_1 = \frac{1}{2} \sum_{\mathbf{k} \in \mathbb{K}_1} \mathcal{E}^{(1)}_{\mathbf{k}} e^{i\theta_{\mathbf{k}}}, \tag{20}$$

where $\mathcal{E}^{(1)}_{\mathbf{k}}(t_{(1)}, \mathbf{x}_{(1)}; t_{(2)}, \mathbf{x}_{(2)}; \ldots)$ is the slowly varying complex wave amplitude, and $\theta_{\mathbf{k}} = \mathbf{k} \cdot \mathbf{x}_{(0)} - \omega_{\mathbf{k}} t_{(0)}$ is the fast varying wave phase. The summation of wave vector $\mathbf{k}$ is over a discrete spectrum $\mathbb{K}_1$. In order for $\mathbf{E}_1 \in \mathbb{R}^3$ to be a real vector, whenever $\mathbf{k} \in \mathbb{K}_1$ is in the spectrum, then $-\mathbf{k}$ must also be in the spectrum. Moreover, the amplitude $\mathcal{E}^{(1)}_{\mathbf{k}}$ must satisfy the reality condition $\mathcal{E}^{(1)}_{-\mathbf{k}} = \mathcal{E}^{(1)*}_{\mathbf{k}}$. Therefore, it is natural to introduce notations

$$\mathbf{z}_{-\mathbf{k}} = \mathbf{z}^*_{\mathbf{k}}, \tag{21}$$

$$\alpha_{-\mathbf{k}} = -\alpha_{\mathbf{k}}, \tag{22}$$

for any complex vector $\mathbf{z} \in \mathbb{C}^3$ and real scalar $\alpha \in \mathbb{R}$ that are labeled by subscript $\mathbf{k}$. For example, the complex vector $\mathcal{E}_{-\mathbf{k}} = \mathcal{E}^*_{\mathbf{k}}$, and the real scalar $\theta_{-\mathbf{k}} = -\theta_{\mathbf{k}}$. Using the above notations, the reality condition is conveniently built into the symbols. In spectral expansion (20), it is tempting to write the summation over discrete wave vector $\mathbf{k}$ as an integral over some continuous spectrum. However, such a treatment will be very cumbersome due to double counting because wave amplitude $\mathcal{E}_{\mathbf{k}}$, which can vary on slow spatial and temporal scales, already has a spectral width.

The first order magnetic field $\mathbf{B}_1$, velocity field $\mathbf{v}_{s1}$, and density field n_{s1} can be expressed in terms of the first order electric field $\mathbf{E}_1$. Substituting expression (20) for the electric field into the first order fluid-Maxwell equations (15)–(17), we immediately find

$$\mathbf{B}_1 = \frac{1}{2} \sum_{\mathbf{k} \in \mathbb{K}_1} \frac{\mathbf{k} \times \mathcal{E}^{(1)}_{\mathbf{k}}}{\omega_{\mathbf{k}}} e^{i\theta_{\mathbf{k}}}, \tag{23}$$

$$\mathbf{v}_{s1} = \frac{ie_s}{2m_s} \sum_{\mathbf{k} \in \mathbb{K}_1} \frac{\mathbb{F}_{s,\mathbf{k}} \mathcal{E}^{(1)}_{\mathbf{k}}}{\omega_{\mathbf{k}}} e^{i\theta_{\mathbf{k}}}, \tag{24}$$

$$n_{s1} = \frac{ie_s n_{s0}}{2m_s} \sum_{\mathbf{k} \in \mathbb{K}_1} \frac{\mathbf{k} \cdot \mathbb{F}_{s,\mathbf{k}} \mathcal{E}^{(1)}_{\mathbf{k}}}{\omega^2_{\mathbf{k}}} e^{i\theta_{\mathbf{k}}}. \tag{25}$$

Here, we introduce the forcing operator $\mathbb{F}_{s,\mathbf{k}} : \mathbb{C}^3 \to \mathbb{C}^3$, acting on any complex vector $\mathbf{z} \in \mathbb{C}^3$ by

$$\mathbb{F}_{s,\mathbf{k}} \mathbf{z} := \gamma^2_{s,\mathbf{k}} \big[\mathbf{z} + i\beta_{s,\mathbf{k}} \mathbf{z} \times \mathbf{b} - \beta^2_{s,\mathbf{k}} (\mathbf{z} \cdot \mathbf{b}) \mathbf{b}\big]. \tag{26}$$

In the above definition, $\mathbf{b}$ is the unit vector in the $\mathbf{B}_0$ direction, $\gamma^2_{s,\mathbf{k}} := 1/(1 - \beta^2_{s,\mathbf{k}})$ is the magnetization factor, $\beta_{s,\mathbf{k}} := \Omega_s/\omega_{\mathbf{k}}$ is the magnetization ratio, and $\Omega_s = e_s B_0/m_s$ is the gyrofrequency of species s. It is clear from Eq. (24) that the forcing operator $\mathbb{F}_{s,\mathbf{k}}$ is related to the linear electric susceptibility $\chi_{s,\mathbf{k}}$ by

$$\chi_{s,\mathbf{k}} = -\frac{\omega^2_{ps}}{\omega^2_{\mathbf{k}}} \mathbb{F}_{s,\mathbf{k}}, \tag{27}$$

where $\omega^2_{ps} = e_s^2 n_{s0}/\epsilon_0 m_s$ is the plasma frequency of species s. While the susceptibility $\chi_{s,\mathbf{k}}$ is typically used in linear theories, the forcing operator $\mathbb{F}_{s,\mathbf{k}}$ will be much more convenient when we discuss nonlinear effects. Note that in the limit $B_0 \to 0$, the forcing operator $\mathbb{F}_{s,\mathbf{k}} \to \mathbf{I}$ becomes the identity operator, and χ_s becomes the cold unmagnetized susceptibility.

The forcing operator $\mathbb{F}_{s,\mathbf{k}}$ will be extremely useful later on when we solve the second order equations. Therefore, let us observe a number of important properties of this operator. For brevity, we will suppress the subscripts s,$\mathbf{k}$, with the implied understanding that all quantities have the same subscripts. First, the operator satisfies the vector identity

$$\mathbb{F}\mathbf{z} = \mathbf{z} + i\beta(\mathbb{F}\mathbf{z}) \times \mathbf{b}. \tag{28}$$

This identity guarantees that the velocity field $\mathbf{v}_{s1}$, given by Eq. (24), satisfies the first order momentum equation (16). Second, $\mathbb{F}$ is a self-adjoint operator with respect to the inner product $\langle \mathbf{w},\mathbf{z}\rangle := \mathbf{w}^\dagger \mathbf{z}$,

$$\mathbf{w}^\dagger \mathbb{F}\mathbf{z} = (\mathbb{F}\mathbf{w})^\dagger \mathbf{z}, \tag{29}$$

for all complex vectors $\mathbf{z},\mathbf{w} \in \mathbb{C}^3$. Using this property, we can move $\mathbb{F}$ from acting on one vector to acting on the other vector in an inner product pair. Third, it is a straightforward calculation to show that

$$\mathbb{F}^2 = \mathbb{F} - \omega \frac{\partial \mathbb{F}}{\partial \omega}, \tag{30}$$

where the dependence of $\mathbb{F}$ on ω comes from β and γ in definition (26). Indeed, using its definition, $\mathbb{F}$ satisfies an obvious identity

$$\mathbb{F}(-\omega) = \mathbb{F}^*(\omega), \tag{31}$$

which can also be written as $\mathbb{F}_{-\mathbf{k}} = \mathbb{F}^*_{\mathbf{k}}$. Lastly, when two frequencies ω_1 and ω_2 are involved, we have a nontrivial quadratic identity

$$(\beta_1 - \beta_2)\mathbb{F}_1\mathbb{F}_2 = \beta_1\mathbb{F}_1 - \beta_2\mathbb{F}_2, \tag{32}$$

which can be shown by straightforward calculation. Using this identity, we can reduce higher powers of the forcing operators to their linear combinations. Combining with property (31), the above identity can generate a number of other similar identities. Properties (28)–(32) will enable important simplifications when we solve the second order equations.

Having expressed other first order perturbations in terms of $\mathbf{E}_1$, the electric field equation (18) constrains the relations between the wave amplitude $\mathcal{E}^{(1)}_{\mathbf{k}}$, the wave frequency $\omega_{\mathbf{k}}$, and the wave vector $\mathbf{k}$. Substituting the expression (16) for $\mathbf{v}_{s1}$ into the electric field equation, we obtain the first order electric field equation in the momentum space

$$\omega^2_{\mathbf{k}}\mathcal{E}^{(1)}_{\mathbf{k}} + c^2\mathbf{k}\times\left(\mathbf{k}\times\mathcal{E}^{(1)}_{\mathbf{k}}\right) = \sum_s \omega^2_{ps}\mathbb{F}_{s,\mathbf{k}}\mathcal{E}^{(1)}_{\mathbf{k}}, \tag{33}$$

which must be satisfied for individual wave vector $\mathbf{k}$ in the spectrum. The above equation can be written in a matrix form $\mathbb{D}_{\mathbf{k}}\mathcal{E}^{(1)}_{\mathbf{k}} = 0$, where the dispersion tensor

$$\mathbb{D}^{ij}_{\mathbf{k}} := \left(\omega^2_{\mathbf{k}} - c^2\mathbf{k}^2\right)\delta^{ij} + c^2k^ik^j - \sum_s \omega^2_{ps}\mathbb{F}^{ij}_{s,\mathbf{k}}. \tag{34}$$

The matrix equation has nontrivial solutions when the wave vector $\mathbf{k}$ and wave frequency $\omega_{\mathbf{k}}$ are such that the linear dispersion relation $\det\mathbb{D}(\mathbf{k},\omega_{\mathbf{k}}) = 0$ is satisfied. When the dispersion relation is indeed satisfied, solving the matrix equation gives wave polarizations. It is well known that in magnetized plasmas, the eigenmodes are two mostly electromagnetic waves and a number of mostly electrostatic hybrid waves. In Appendix B, we review the dispersion relations and wave polarizations when waves propagate at arbitrary angles with respect to the background magnetic field.

Finally, to introduce one more operator that will be useful for solving the second order equations, let us calculate the wave energy. The average energy carried by linear waves can be found by summing up average energy carried by fields and particles. For a single linear wave with wave vector $\mathbf{k}$, after averaging on $t_{(0)}$ and $\mathbf{x}_{(0)}$ scale, the wave energy

$$\begin{aligned} U_{\mathbf{k}} &= \frac{\epsilon_0}{2}\langle\mathbf{E}^2_1\rangle_{(0)} + \frac{1}{2\mu_0}\langle\mathbf{B}^2_1\rangle_{(0)} + \frac{1}{2}\sum_s n_{s0}m_s\langle\mathbf{v}^2_{s1}\rangle_{(0)} \\ &= \frac{\epsilon_0}{4}\mathcal{E}^{(1)*}_{\mathbf{k}}\cdot\mathbb{H}_{\mathbf{k}}\mathcal{E}^{(1)}_{\mathbf{k}}, \end{aligned} \tag{35}$$

where we introduce the normalized wave energy operator

$$\mathbb{H}_{\mathbf{k}} := 2\mathbb{I} - \sum_s \frac{\omega^2_{ps}}{\omega_{\mathbf{k}}}\frac{\partial\mathbb{F}_{s,\mathbf{k}}}{\partial\omega_{\mathbf{k}}} = \frac{1}{\omega_{\mathbf{k}}}\frac{\partial\left(\omega^2_{\mathbf{k}}\epsilon_{\mathbf{k}}\right)}{\partial\omega_{\mathbf{k}}}. \tag{36}$$

Here, $\epsilon_{\mathbf{k}} = \mathbb{I} + \sum_s \chi_{s,\mathbf{k}}$ is the dielectric tensor, and we have used Eq. (27), which relates the forcing operator to the susceptibility. When evaluating $\langle\mathbf{B}^2_1\rangle$, we have used expression (23) for $\mathbf{B}_1$, followed by simplification using the momentum space electric field equation (33). This term is then combined with $\langle\mathbf{v}^2_{s1}\rangle$, calculated using Eq. (24) for $\mathbf{v}_{s1}$. The final result is simplified using identity (30) for the forcing operator $\mathbb{F}_{s,\mathbf{k}}$. Now that we have introduced the wave energy operator $\mathbb{H}_{\mathbf{k}}$, the momentum space electric field equation (33) can be converted into a form that is closely related to the wave energy

$$\frac{\partial\omega_{\mathbf{k}}}{\partial k_l}\omega_{\mathbf{k}}\mathbb{H}^{ij}_{\mathbf{k}}\mathcal{E}^{(1)j}_{\mathbf{k}} = c^2(2k_l\delta_{ij} - k_i\delta_{jl} - k_j\delta_{il})\mathcal{E}^{(1)j}_{\mathbf{k}}. \tag{37}$$

This form of the first order electric field equation is obtained by taking $\partial/\partial k_l$ derivative on both sides of Eq. (33). Notice that although $\mathcal{E}^{(1)}_{\mathbf{k}}$ is labeled by $\mathbf{k}$, it does not explicitly depend on $\mathbf{k}$. This alternative form of the first order electric field equation will be useful when we solve the second order equations.

B. Second order equations

To obtain the second order equations, we collect all the $O(\lambda^2)$ terms in the asymptotic expansions. The resultant second order equations are

$$\partial_{t(0)}\mathbf{B}_2 = -\partial_{t(1)}\mathbf{B}_1 - \boldsymbol{\nabla}_{(1)}\times\mathbf{E}_1 - \boldsymbol{\nabla}_{(0)}\times\mathbf{E}_2, \tag{38}$$

$$\begin{aligned} \partial_{t(0)}\mathbf{v}_{s2} = &-\partial_{t(1)}\mathbf{v}_{s1} - \mathbf{v}_{s1}\cdot\boldsymbol{\nabla}_{(0)}\mathbf{v}_{s1} \\ &+ \frac{e_s}{m_s}(\mathbf{v}_{s1}\times\mathbf{B}_1 + \mathbf{E}_2 + \mathbf{v}_{s2}\times\mathbf{B}_0), \end{aligned} \tag{39}$$

$$\begin{aligned} \partial_{t(0)}n_{s2} = &-\partial_{t(1)}n_{s1} - \boldsymbol{\nabla}_{(0)}\cdot(n_{s1}\mathbf{v}_{s1}) \\ &- n_{s0}(\boldsymbol{\nabla}_{(1)}\cdot\mathbf{v}_{s1} + \boldsymbol{\nabla}_{(0)}\cdot\mathbf{v}_{s2}), \end{aligned} \tag{40}$$

$$\begin{aligned} \Box^{(0)}_{ij}E^j_2 = &-\Box^{(1)}_{ij}E^j_1 - \frac{1}{\epsilon_0}\sum_s e_s\big[n_{s0}\partial_{t(1)}v^i_{s1} \\ &+ \partial_{t(0)}\left(n_{s1}v^i_{s1}\right) + n_{s0}\partial_{t(0)}v^i_{s2}\big]. \end{aligned} \tag{41}$$

Again, the electric field equation (41) is obtained by substituting Faraday's law into the Maxwell-Ampère's equation. In doing so, we introduce the first order differential operator

$$\begin{aligned} \Box^{(1)}_{ij} := &2\left(\partial_{t(0)}\partial_{t(1)} - c^2\partial^{(0)}_l\partial^{(1)}_l\right)\delta_{ij} \\ &+ c^2\left(\partial^{(0)}_i\partial^{(1)}_j + \partial^{(1)}_i\partial^{(0)}_j\right). \end{aligned} \tag{42}$$

This operator mixes fast and slow scales, and will govern how wave amplitudes vary on the slow scales due to interactions that happen on the fast scale.

To solve the second order equations, notice that although the second order equations are nonlinear in $\mathbf{B}_1$, $\mathbf{v}_{s1}$, and n_{s1}, they are nevertheless linear in $\mathbf{E}_2$, $\mathbf{B}_2$, $\mathbf{v}_{s2}$, and n_{s2}. Therefore, we may solve for the second order perturbations from the linear equations, regarding nonlinearities in first order perturbations as source terms. The general solution to such a system of linear equations is again a superposition of plane waves. Let us write the second order electric field

$$\mathbf{E}_2 = \frac{1}{2}\sum_{\mathbf{k}\in\mathbb{K}_2} \mathcal{E}^{(2)}_{\mathbf{k}} e^{i\theta_{\mathbf{k}}}. \tag{43}$$

Similar to the first order expansion (20), in the above expression, $\mathcal{E}^{(2)}_{\mathbf{k}}(t_{(1)},\mathbf{x}_{(1)};t_{(2)},\mathbf{x}_{(2)};\dots)$ is the second order slowly varying complex wave amplitude, $\theta_{\mathbf{k}}$ is the fast wave phase, and $\mathbb{K}_2$ is the spectrum of second order fluctuations, which contains $-\mathbf{k}$ whenever $\mathbf{k}\in\mathbb{K}_2$. The second order spectrum $\mathbb{K}_2$ is highly constrained and will need to be determined from the second order electric field equation, once the first order spectrum $\mathbb{K}_1$ is given.

Before we can determine $\mathbb{K}_2$ and $\mathcal{E}^{(2)}_{\mathbf{k}}$, we need to express $\mathbf{B}_2$ in terms of $\mathbf{E}_2$. Plugging in expressions for the first order fluctuations (20) and (23) into the second order Faraday's law (38), the second order magnetic field can be expressed as

$$\begin{aligned}\mathbf{B}_2 = {}& \frac{1}{2}\sum_{\mathbf{k}\in\mathbb{K}_2} \frac{\mathbf{k}\times\mathcal{E}^{(2)}_{\mathbf{k}}}{\omega_{\mathbf{k}}} e^{i\theta_{\mathbf{k}}} \\ & + \frac{1}{2}\sum_{\mathbf{k}\in\mathbb{K}_1}\left(\frac{\boldsymbol{\nabla}_{(1)}\times\mathcal{E}^{(1)}_{\mathbf{k}}}{i\omega_{\mathbf{k}}} + \frac{\mathbf{k}\times\partial_{t(1)}\mathcal{E}^{(1)}_{\mathbf{k}}}{i\omega^2_{\mathbf{k}}}\right)e^{i\theta_{\mathbf{k}}}.\end{aligned} \tag{44}$$

The first line has the same structure as $\mathbf{B}_1$, except now the summation is over the second order spectrum $\mathbb{K}_2$. The second line involves slow derivatives of the first order amplitude $\mathcal{E}^{(1)}_{\mathbf{k}}$. These derivatives, still unknown at this step, will be determined later from the second order electric field equation.

Similarly, the second order velocity $\mathbf{v}_{s2}$ can be solved from Eq. (39). One way of solving this equation is by first taking the Fourier transform on $t_{(0)}$ and $\mathbf{x}_{(0)}$ scale. Then, in the Fourier space, the resultant algebraic equation can be readily solved using the property (28) of the forcing operator. After taking the inverse Fourier transform, the second order velocity can be expressed as

$$\begin{aligned}\mathbf{v}_{s2} = {}& \frac{ie_s}{2m_s}\sum_{\mathbf{k}\in\mathbb{K}_2}\frac{\mathbb{F}_{s,\mathbf{k}}\mathcal{E}^{(2)}_{\mathbf{k}}}{\omega_{\mathbf{k}}}e^{i\theta_{\mathbf{k}}} \\ & + \frac{e_s}{2m_s}\sum_{\mathbf{k}\in\mathbb{K}_1}\frac{\mathbb{F}^2_{s,\mathbf{k}}\partial_{t(1)}\mathcal{E}^{(1)}_{\mathbf{k}}}{\omega^2_{\mathbf{k}}}e^{i\theta_{\mathbf{k}}} \\ & - \frac{e_s^2}{4m_s^2}\sum_{\mathbf{q},\mathbf{q}'\in\mathbb{K}_1}\frac{\mathbb{F}_{s,\mathbf{q}+\mathbf{q}'}\left(\mathbf{L}^s_{\mathbf{q},\mathbf{q}'}+\mathbf{T}^s_{\mathbf{q},\mathbf{q}'}\right)}{\omega_{\mathbf{q}}+\omega'_{\mathbf{q}}}e^{i\theta_{\mathbf{q}}+i\theta_{\mathbf{q}'}}.\end{aligned} \tag{45}$$

The first two lines of the above expression is in analogy to the expression (44) for $\mathbf{B}_2$. The third line comes from beating of nonlinearities. In particular, the $\mathbf{v}_{s1}\times\mathbf{B}_1$ nonlinearity introduces a longitudinal beating

$$\mathbf{L}^s_{\mathbf{q},\mathbf{q}'} = \frac{\left(\mathbb{F}_{s,\mathbf{q}}\mathcal{E}^{(1)}_{\mathbf{q}}\right)\times\left(\mathbf{q}'\times\mathcal{E}^{(1)}_{\mathbf{q}'}\right)}{\omega_{\mathbf{q}}\omega_{\mathbf{q}'}}. \tag{46}$$

In addition, the Euler derivative $\mathbf{v}_{s1}\cdot\boldsymbol{\nabla}_{(0)}\mathbf{v}_{s1}$, which is responsible for generating turbulence in neutral fluids, gives rise to a turbulent beating

$$\mathbf{T}^s_{\mathbf{q},\mathbf{q}'} = \frac{\left(\mathbb{F}_{s,\mathbf{q}}\mathcal{E}^{(1)}_{\mathbf{q}}\right)\left(\mathbf{q}\cdot\mathbb{F}_{s,\mathbf{q}'}\mathcal{E}^{(1)}_{\mathbf{q}'}\right)}{\omega_{\mathbf{q}}\omega_{\mathbf{q}'}}. \tag{47}$$

The third line in Eq. (45) may be simplified using the quadratic property (32) of the forcing operator. This simplification will be done later when we discuss interaction of three waves in the next section.

Using similar method, we can find the expression for the second order density n_{s2}. Although the expression for n_{s2} is not indispensable for studying three-wave scattering, we present it here because it will become useful when one studies four-wave or even higher order interactions. The second order density can be expressed as

$$\begin{aligned}n_{s2} = {}& \frac{e_s n_{s0}}{2m_s}\left[\sum_{\mathbf{k}\in\mathbb{K}_2}\frac{i\mathbf{k}\cdot\mathbb{F}_{s,\mathbf{k}}\mathcal{E}^{(2)}_{\mathbf{k}}}{\omega^2_{\mathbf{k}}}e^{i\theta_{\mathbf{k}}}\right. \\ & \left. + \sum_{\mathbf{k}\in\mathbb{K}_1}\left(\frac{\mathbf{k}\cdot\left(\mathbb{F}_{s,\mathbf{k}}+\mathbb{F}^2_{s,\mathbf{k}}\right)\partial_{t(1)}\mathcal{E}^{(1)}_{\mathbf{k}}}{\omega^3_{\mathbf{k}}} + \frac{\boldsymbol{\nabla}_{(1)}\cdot\mathbb{F}_{s,\mathbf{k}}\mathcal{E}^{(1)}_{\mathbf{k}}}{\omega^2_{\mathbf{k}}}\right)e^{i\theta_{\mathbf{k}}}\right] \\ & - \frac{e_s^2 n_{s0}}{4m_s^2}\sum_{\mathbf{q},\mathbf{q}'\in\mathbb{K}_1}\frac{(\mathbf{q}+\mathbf{q}')\cdot\mathbf{R}^s_{\mathbf{q},\mathbf{q}'}}{(\omega_{\mathbf{q}}+\omega'_{\mathbf{q}})^2}e^{i\theta_{\mathbf{q}}+i\theta_{\mathbf{q}'}}.\end{aligned} \tag{48}$$

The above three lines are in analogy to those for $\mathbf{v}_{s2}$ in Eq. (45). In the third line, the quadratic response

$$\mathbf{R}^s_{\mathbf{q},\mathbf{q}'} = \mathbb{F}_{s,\mathbf{q}+\mathbf{q}'}\left(\mathbf{L}^s_{\mathbf{q},\mathbf{q}'}+\mathbf{T}^s_{\mathbf{q},\mathbf{q}'}\right) + \left(1+\frac{\omega_{\mathbf{q}}}{\omega'_{\mathbf{q}}}\right)\mathbf{C}^s_{\mathbf{q},\mathbf{q}'}, \tag{49}$$

where the longitudinal beating $\mathbf{L}^s_{\mathbf{q},\mathbf{q}'}$ and the turbulent beating $\mathbf{T}^s_{\mathbf{q},\mathbf{q}'}$ are given by Eqs. (46) and (47). The third term, proportional to $\mathbf{C}^s_{\mathbf{q},\mathbf{q}'}$, comes from the divergence of the nonlinear current $\boldsymbol{\nabla}_{(0)}\cdot(n_{s1}\mathbf{v}_{s1})$, which introduces the current beating

$$\mathbf{C}^s_{\mathbf{q},\mathbf{q}'} = \frac{\left(\mathbb{F}_{s,\mathbf{q}}\mathcal{E}^{(1)}_{\mathbf{q}}\right)\left(\mathbf{q}'\cdot\mathbb{F}_{s,\mathbf{q}'}\mathcal{E}^{(1)}_{\mathbf{q}'}\right)}{\omega_{\mathbf{q}}\omega_{\mathbf{q}'}}. \tag{50}$$

Notice here the inner product is with $\mathbf{q}'$, in contrast to turbulent beating $\mathbf{T}^s_{\mathbf{q},\mathbf{q}'}$, in which the inner product is with $\mathbf{q}$ instead. This makes the physics of these two types of beating fundamentally different.

Having expressed second order fluctuations in terms of $\mathbf{E}_2$, we can obtain an equation that only involves electric perturbations. Substituting expressions (24), (25), and (45) into the second order electric field equation (41), we can eliminate $\mathbf{v}_{s1}$, n_{s1}, and $\mathbf{v}_{s2}$. The resultant equation can be simplified using the first order electric field equation (37), as well as property (30) of the forcing operator. The second order electric field equation can then be put into a rather simple and intuitive

form

$$\sum_{\mathbf{k}\in\mathbb{K}_2} \mathbb{D}_{\mathbf{k}}\mathcal{E}^{(2)}_{\mathbf{k}} e^{i\theta_{\mathbf{k}}} + i\sum_{\mathbf{k}\in\mathbb{K}_1} \omega_{\mathbf{k}}\mathbb{H}_{\mathbf{k}} d^{\mathbf{k}}_{t(1)}\mathcal{E}^{(1)}_{\mathbf{k}} e^{i\theta_{\mathbf{k}}} = \frac{i}{2}\sum_{s,\mathbf{q},\mathbf{q}'\in\mathbb{K}_1} \mathbf{S}^s_{\mathbf{q},\mathbf{q}'} e^{i\theta_{\mathbf{q}}+i\theta_{\mathbf{q}'}}. \tag{51}$$

The left-hand side is a modification of the first order spectrum, as consequences of three-wave scattering on the right-hand side. In the above equation, the dispersion tensor $\mathbb{D}_{\mathbf{k}} = \mathbb{D}^*_{-\mathbf{k}}$ is defined by Eq. (34), the normalized wave energy operator $\mathbb{H}_{\mathbf{k}} = \mathbb{H}^*_{-\mathbf{k}}$ is defined by Eq. (36), and $d^{\mathbf{k}}_{t(1)} = d^{-\mathbf{k}}_{t(1)}$ is the advective derivative

$$d^{\mathbf{k}}_{t(1)} := \partial_{t(1)} + \frac{\partial\omega_{\mathbf{k}}}{\partial\mathbf{k}}\cdot\nabla_{(1)}, \tag{52}$$

which advects the wave envelope at the wave group velocity $\mathbf{v}_g = \partial\omega_{\mathbf{k}}/\partial\mathbf{k}$ on the slow scale $t_{(1)}$ and $\mathbf{x}_{(1)}$. In Eq. (51), the three-wave scattering strength

$$\mathbf{S}^s_{\mathbf{q},\mathbf{q}'} = \frac{e_s\omega^2_{ps}}{2m_s}\left(\mathbf{R}^s_{\mathbf{q},\mathbf{q}'} + \mathbf{R}^s_{\mathbf{q}',\mathbf{q}}\right), \tag{53}$$

where the quadratic response $\mathbf{R}^s_{\mathbf{q},\mathbf{q}'}$ is given by Eq. (49). Notice that the scattering strength $\mathbf{S}^s_{\mathbf{q},\mathbf{q}'}$ is proportional to the density n_{s0}. This is intuitive because three-wave scattering cannot happen in vacuum. Hence, all three-wave scatterings come from charged particle response, which is additive and therefore proportional to the density. Also notice that $\mathbf{S}^s_{\mathbf{q},\mathbf{q}'}$ is proportional to the charge-to-mass ratio. This is also intuitive because e_s/m_s is the coefficient by which charged particles respond to the electric field.

Let us observe a number of properties of the scattering strength $\mathbf{S}^s_{\mathbf{q},\mathbf{q}'}$. First, by construction, the scattering strength is symmetric with respect to $\mathbf{q},\mathbf{q}'$, namely,

$$\mathbf{S}^s_{\mathbf{q},\mathbf{q}'} = \mathbf{S}^s_{\mathbf{q}',\mathbf{q}}. \tag{54}$$

In addition, using notations (21) and (22), it is easy to see that reality condition for $\mathbf{S}_{\mathbf{q},\mathbf{q}'}$ is

$$\mathbf{S}^{s*}_{\mathbf{q},\mathbf{q}'} = -\mathbf{S}^s_{-\mathbf{q},-\mathbf{q}'}. \tag{55}$$

Moreover, it turns out that the scattering strength $\mathbf{S}^s_{\mathbf{q},\mathbf{q}'}$ satisfies the important identity

$$\mathbf{S}^s_{\mathbf{q},-\mathbf{q}} = \mathbf{0}. \tag{56}$$

This identity can be shown by straightforward calculation using the limiting form $\mathbb{F}(\omega)\to\mathbf{bb}$ when $\omega\to 0$. Identity (56) guarantees that no zero-frequency mode with $\omega_{\mathbf{k}} = 0$ will arise in the second order electric field equation. Without this important identity, any change in the wave amplitude would be faster then the zero-frequency mode, a situation that would violate the multiscale assumption. Fortunately, due to identity (56), the multiscale perturbative solution is well justified.

Now that we have obtained the second order electric field equation (51), we can use it to constrain the spectrum $\mathbb{K}_2$ and the amplitude $\mathcal{E}^{(2)}_{\mathbf{k}}$. In order to satisfy (51), the coefficient of each Fourier exponent $e^{i\theta_{\mathbf{k}}}$ must be matched on both sides of the equation. To match the spectrum on the right-hand side of Eq. (51), which is generated by beating of first order perturbations, we can take the second order spectrum to be

$$\mathbb{K}_2 = \left(\mathbb{K}^0_1 \bigoplus \mathbb{K}^0_1\right)\setminus\mathbb{K}^0_1, \tag{57}$$

where the set $\mathbb{K}^0_1 := \mathbb{K}_1\bigcup\{\mathbf{0}\}$. We define the direct sum of two sets $G_1, G_2\subseteq G$, where G is an additive group, by $G_1\bigoplus G_2 := \{g_1+g_2 | g_1\in G_1, g_2\in G_2\}$. We can exclude the zero vector $\mathbf{0}$ from the second order spectrum $\mathbb{K}_2$ using property (56) of the scattering strength. We also excluded vectors that are already contained in the first order spectrum $\mathbb{K}_1$, such that the matrix $\mathbb{D}_{\mathbf{k}}$ is invertible for all $\mathbf{k}\in\mathbb{K}_2$. Since the matrix is invertible, the second order amplitude $\mathcal{E}^{(2)}_{\mathbf{k}}$ is determined by

$$\mathcal{E}^{(2)}_{\mathbf{k}} = i\mathbb{D}^{-1}_{\mathbf{k}}\sum_s \mathbf{S}^s_{\mathbf{q},\mathbf{q}'}, \tag{58}$$

where $\mathbf{q},\mathbf{q}'\in\mathbb{K}_1$ are such that $\mathbf{k} = \mathbf{q}+\mathbf{q}'\in\mathbb{K}_2$. Here, the factor $\frac{1}{2}$ has been removed using the symmetry property $2\mathbf{S}^s_{\mathbf{q},\mathbf{q}'} = \mathbf{S}^s_{\mathbf{q},\mathbf{q}'} + \mathbf{S}^s_{\mathbf{q}',\mathbf{q}}$. We can put the above abstract notations in more intuitive language as follows. The first order spectrum contains all the "on-shell" waves, which satisfy the dispersion relation $\det\mathbb{D}(\mathbf{k},\omega_{\mathbf{k}}) = 0$ for all $\mathbf{k}\in\mathbb{K}_1$, while the second order spectrum $\mathbb{K}_2$ contains all the "off-shell" waves. These "off-shell" quasimodes do not satisfy the linear dispersion relation, and their amplitude is driven by the beating of two "on-shell" waves.

To illustrate the abstract notations introduced above, let us consider the simplest example where the spectrum $\mathbb{K}_1$ contains only one "on-shell" wave, namely, $\mathbb{K}_1 = \{\mathbf{k},-\mathbf{k}\}$. In this case, the second order spectrum $\mathbb{K}_2 = \{2\mathbf{k},-2\mathbf{k}\}$ contains the second harmonic. Matching the Fourier exponents, the "on-shell" equation is

$$\omega_{\mathbf{k}}\mathbb{H}_{\mathbf{k}} d^{\mathbf{k}}_{t(1)}\mathcal{E}^{(1)}_{\mathbf{k}} = \mathbf{0}. \tag{59}$$

The other "on-shell" equation is the complex conjugate of the above equation. Since $\mathbb{H}_{\mathbf{k}}$ enters the wave energy (35), this matrix is positive definite and therefore nondegenerate. Hence, the above equation can be written as $d^{\mathbf{k}}_{t(1)}\mathcal{E}^{(1)}_{\mathbf{k}} = \mathbf{0}$, which says that the wave amplitude is a constant of advection. Next, matching coefficients of the other Fourier exponent, we obtain the "off-shell" equation for the second harmonic

$$\mathbb{D}_{2\mathbf{k}}\mathcal{E}^{(2)}_{2\mathbf{k}} = i\sum_s \mathbf{S}^s_{\mathbf{k},\mathbf{k}}. \tag{60}$$

After inverting the matrix $\mathbb{D}_{2\mathbf{k}}$, this equation gives the amplitude of the second harmonic in terms of the amplitude of the first harmonic. Moreover, since the complex amplitude $\mathcal{E}^{(2)}_{2\mathbf{k}}$ also encodes the phase information, the above equation also tells how the second harmonic is phase locked with the fundamental.

III. SCATTERING OF THREE RESONANT ON-SHELL WAVES

In this section, we illustrate the general theory developed in Sec. II with the simplest nontrivial example where the spectrum contains exactly three resonant "on-shell" waves. Without loss of generality, suppose the three waves satisfy the

resonance conditions

$$\mathbf{k}_1 = \mathbf{k}_2 + \mathbf{k}_3, \tag{61}$$

$$\omega_{\mathbf{k}_1} = \omega_{\mathbf{k}_2} + \omega_{\mathbf{k}_3}, \tag{62}$$

where all ω's are positive. The above resonance condition can also be written more compactly as $\theta_{\mathbf{k}_1} = \theta_{\mathbf{k}_2} + \theta_{\mathbf{k}_3}$. In this case, the spectrum $\mathbb{K}_1 = \{\mathbf{k}_1, \mathbf{k}_2, \mathbf{k}_3, (\mathbf{k} \to -\mathbf{k})\}$. Using Eq. (57), we find the second order spectrum $\mathbb{K}_2 = \{2\mathbf{k}_1, 2\mathbf{k}_2, 2\mathbf{k}_3, \mathbf{k}_1 + \mathbf{k}_2, \mathbf{k}_2 - \mathbf{k}_3, \mathbf{k}_3 + \mathbf{k}_1, (\mathbf{k} \to -\mathbf{k})\}$. Notice that resonant waves, such as $\mathbf{k}_1 = \mathbf{k}_2 + \mathbf{k}_3$, are not contained in the second order spectrum $\mathbb{K}_2$. In this way, we avoid the ambiguous partition between $\mathcal{E}^{(2)}_{\mathbf{k}}$, and $d^{\mathbf{k}}_{t(1)}\mathcal{E}^{(1)}_{\mathbf{k}}$. In other words, all perturbative corrections to the first order amplitude $\mathcal{E}^{(1)}_{\mathbf{k}}$ are accounted for by its slow derivatives.

Using the electric field equation (51), we can extract the "off-shell" equations by matching coefficients of Fourier exponents. There are 12 "off-shell" equations, appearing in 6 conjugate pairs. Among these, three pairs govern the production of second harmonics $2\mathbf{k}_1$, $2\mathbf{k}_2$, and $2\mathbf{k}_3$. For example,

$$\mathbb{D}_{2\mathbf{k}_1}\mathcal{E}^{(2)}_{2\mathbf{k}_1} = i\sum_s \mathbf{S}^s_{\mathbf{k}_1,\mathbf{k}_1}. \tag{63}$$

The other three pairs of equations govern to production of "off-shell" beatings. For example,

$$\mathbb{D}_{\mathbf{k}_1+\mathbf{k}_2}\mathcal{E}^{(2)}_{\mathbf{k}_1+\mathbf{k}_2} = i\sum_s \mathbf{S}^s_{\mathbf{k}_1,\mathbf{k}_2}. \tag{64}$$

Similarly, we have equations governing the $\mathbf{k}_2 - \mathbf{k}_3$ and $\mathbf{k}_3 + \mathbf{k}_1$ quasimodes. Since the dispersion tensor $\mathbb{D}_{\mathbf{q}}$ for any "off-shell" quasimode is nondegenerate, the second order amplitudes $\mathcal{E}^{(2)}_{\mathbf{k}}$ can be found by simply inverting the above matrix equations, which give the second order amplitudes in terms of the first order amplitudes.

Similarly, we can extract the on-shell equations from the second order electric field equation (51). There are six on-shell equations, three of which are complex conjugation of the following three on-shell equations:

$$\omega_1\mathbb{H}_1 d_t\mathcal{E}_1 = \sum_s \mathbf{S}^s_{2,3}, \tag{65}$$

$$\omega_2\mathbb{H}_2 d_t\mathcal{E}_2 = \sum_s \mathbf{S}^s_{1,\bar{3}}, \tag{66}$$

$$\omega_3\mathbb{H}_3 d_t\mathcal{E}_3 = \sum_s \mathbf{S}^s_{1,\bar{2}}. \tag{67}$$

Here, we have suppressed subscripts and superscripts whenever sensible, and denoted $-j$ by $\bar{j}$ for the compactness of notations. In the above equations, the left-hand sides are passive advections of wave envelopes at group velocities, while the right-hand sides govern redistribution of wave action due to three-wave scattering.

A. Action conservation of on-shell equations

By the conservative nature of the redistribution process, the on-shell equations (65)–(67) conserve the total wave action U/ω, as well as the total wave energy U. As will be proven in the next paragraph, the local conservation laws of wave actions are

$$d_t\frac{U_1}{\omega_1} + d_t\frac{U_2}{\omega_2} = 0, \tag{68}$$

$$d_t\frac{U_3}{\omega_3} - d_t\frac{U_2}{\omega_2} = 0, \tag{69}$$

where U_j, given by Eq. (35), is the energy of the linear wave with wave vector $\mathbf{k}_j$. The first conservation law (68) implies that the total number of wave quanta in the incident wave and the scattered wave is a constant. This is intuitive because, in the absence of damping, whenever a quanta of the $\mathbf{k}_1$ mode is annihilated, it is consumed to create a quanta of the $\mathbf{k}_2$ mode. Analogously, the second conservation law (69) says that whenever a quanta of the $\mathbf{k}_2$ mode is created, a quanta of the $\mathbf{k}_3$ mode must also be created by the three-wave process (61). As a consequence of wave action conservation, the total wave energy is also conserved during resonant three-wave interaction

$$d_tU_1 + d_tU_2 + d_tU_3 = 0. \tag{70}$$

This local energy conservation law can be obtained by linearly combining Eqs. (68) and (69), and use the frequency resonance condition (62). The conservation of wave energy is also intuitive because in the absence of damping and other waves, three-wave scattering can only redistribute energy among the three waves.

The above conservation laws can be proven by noting the following properties of the scattering strength $\mathbf{S}^s_{\mathbf{q},\mathbf{q}'}$. First, using formula (53) for the scattering strength, together with the quadratic identity (32) of the forcing operator $\mathbb{F}$, we can obtain a simple expression for $\mathbf{S}^s_{\mathbf{k}_2,\mathbf{k}_3}$:

$$\begin{aligned}\mathbf{S}_{2,3} = \frac{e\omega_p^2\omega_1}{2m\omega_2\omega_3}\Bigg[&\frac{(\mathcal{E}_3\cdot\mathbb{F}_2\mathcal{E}_2)(\mathbb{F}_1\mathbf{k}_3)+(\mathcal{E}_2\cdot\mathbb{F}_3\mathcal{E}_3)(\mathbb{F}_1\mathbf{k}_2)}{\omega_1}\\ &+\frac{(\mathbb{F}_3\mathcal{E}_3)(\mathbf{k}_1\cdot\mathbb{F}_2\mathcal{E}_2)-(\mathbb{F}_1\mathcal{E}_3)(\mathbf{k}_3\cdot\mathbb{F}_2\mathcal{E}_2)}{\omega_2}\\ &+\frac{(\mathbb{F}_2\mathcal{E}_2)(\mathbf{k}_1\cdot\mathbb{F}_3\mathcal{E}_3)-(\mathbb{F}_1\mathcal{E}_2)(\mathbf{k}_2\cdot\mathbb{F}_3\mathcal{E}_3)}{\omega_3}\Bigg].\end{aligned} \tag{71}$$

The expression for $\mathbf{S}_{1,\bar{3}}$ can be obtained easily from Eq. (71) using the replacement rule $1 \to 2$, $2 \to 1$, $3 \to -3$, where the minus sign is interpreted using notations (21) and (22). Similarly, to obtain the expression for $\mathbf{S}_{1,\bar{2}}$, we can replace $1 \to 3$, $2 \to 1$, $3 \to -2$ in Eq. (71). Second, having obtained expressions for $\mathbf{S}_{2,3}$, $\mathbf{S}_{1,\bar{3}}$, and $\mathbf{S}_{1,\bar{2}}$, we can use the self-adjoint property (29) of the forcing operator to show, by straightforward calculations, that the scattering strength for three resonant waves satisfies the following identities:

$$\frac{\mathcal{E}_1\cdot\mathbf{S}^*_{2,3}}{\omega_1^2} + \frac{\mathcal{E}_2^*\cdot\mathbf{S}_{1,\bar{3}}}{\omega_2^2} = 0, \tag{72}$$

$$\frac{\mathcal{E}_2^*\cdot\mathbf{S}_{1,\bar{3}}}{\omega_2^2} - \frac{\mathcal{E}_3^*\cdot\mathbf{S}_{1,\bar{2}}}{\omega_3^2} = 0. \tag{73}$$

Then, the action conservation equations (68) and (69), as well as the energy conservation equation (70), are immediate consequences of the above identities.

One may be puzzled by the expression (71) for $\mathbf{S}_{2,3}$. After all, why $\mathbf{S}_{2,3}$ is given by those six particular combinations of vectors $\mathbb{F}_{\mathbf{q}}\mathcal{E}_{\mathbf{q}'}$ and $\mathbb{F}_{\mathbf{q}}\mathbf{q}'$, weighted by inner products $\mathcal{E}_{\mathbf{q}}\cdot\mathbb{F}_{\mathbf{q}'}\mathcal{E}_{\mathbf{q}'}$ and $\mathbf{q}\cdot\mathbb{F}_{\mathbf{q}'}\mathcal{E}_{\mathbf{q}'}$, as well as signed frequencies $\pm 1/\omega$? At first glance, there seems to be no obvious pattern. However, action conservation laws, given by Eqs. (72) and (73), clearly indicate that $\mathbf{S}_{2,3}$, $\mathbf{S}_{1,\bar{3}}$, and $\mathbf{S}_{1,\bar{2}}$ originate from a single term in the variational principle. In Sec. IV, we will write the Lagrangian that generates the three on-shell equations (65)–(67). From the Lagrangian, it will become obvious why Eq. (71) looks the way it is.

B. Three-wave equations

When one is not concerned with the vector dependence of the complex wave amplitude $\mathcal{E}_{\mathbf{k}}$, the on-shell equations (65)–(67) can be written as three scalar equations, called the three-wave equations. To remove the vector dependence, let us decompose $\mathcal{E}_{\mathbf{k}} = \mathbf{e}_{\mathbf{k}}\varepsilon_{\mathbf{k}}$, where $\mathbf{e}_{\mathbf{k}}$ is the complex unit vector satisfying $\mathbf{e}_{\mathbf{k}}^*\cdot\mathbf{e}_{\mathbf{k}} = 1$. This decomposition is not unique due to the U(1) symmetry $\mathbf{e}_{\mathbf{k}} \to e^{i\alpha}\mathbf{e}_{\mathbf{k}}$ and $\varepsilon_{\mathbf{k}} \to e^{-i\alpha}\varepsilon_{\mathbf{k}}$. By requiring the scalar amplitude $\varepsilon_{\mathbf{k}} \in \mathbb{R}$ to be real valued, the symmetry group of the above decomposition is reduced to the $\mathbb{Z}_2$ symmetry $\varepsilon \to -\varepsilon$. The convective derivative of the complex wave amplitude

$$d_t\mathcal{E}_{\mathbf{k}} = \mathbf{e}_{\mathbf{k}}d_t\varepsilon_{\mathbf{k}} + \varepsilon_{\mathbf{k}}d_t\mathbf{e}_{\mathbf{k}}, \tag{74}$$

can be decomposed into change due to the scalar amplitude and the change due to the rotation of the complex unit vector.

The left-hand sides of the on-shell equations are closely related to the energy of the linear waves. Denote the dimensionless wave energy coefficient

$$u_{\mathbf{k}} := \tfrac{1}{2}\mathbf{e}_{\mathbf{k}}^\dagger\mathbb{H}_{\mathbf{k}}\mathbf{e}_{\mathbf{k}}. \tag{75}$$

Then, the wave energy Eq. (35) can be written as $U_{\mathbf{k}} = \epsilon_0 u_{\mathbf{k}}\varepsilon_{\mathbf{k}}^2/2$. Notice that the energy coefficient $u_{\mathbf{k}} > 0$ is always real and positive because the matrix $\mathbb{H}_{\mathbf{k}}$ is Hermitian and positive definite. Taking inner product with $\mathbf{e}_{\mathbf{k}}^*$ on both sides of the on-shell equations and sum the result with its Hermitian conjugate, we obtain $u_{\mathbf{k}}d_t\varepsilon_{\mathbf{k}} + \frac{1}{2}\varepsilon_{\mathbf{k}}d_tu_{\mathbf{k}} = \sum_s[\mathbf{e}_{\mathbf{k}}^\dagger\mathbf{S}_{\mathbf{q},\mathbf{q}'}^s/\omega_{\mathbf{k}} + \text{c.c.}]/4$. From this expression, we see the combination $\varepsilon_{\mathbf{k}}u_{\mathbf{k}}^{1/2}$ will be particularly convenient. Let us nondimensionalize the electric field amplitude by electron mass

$$a_{\mathbf{k}} := \frac{e\varepsilon_{\mathbf{k}}}{m_ec\omega_{\mathbf{k}}}u_{\mathbf{k}}^{1/2}. \tag{76}$$

Then, the on-shell equations can then be written in terms of the normalized wave amplitude $d_ta_{\mathbf{k}} = e/(4m_ec\omega_{\mathbf{k}}u_{\mathbf{k}}^{1/2})\sum_s(\mathbf{e}_{\mathbf{k}}^\dagger\mathbf{S}_{\mathbf{q},\mathbf{q}'}^s/\omega_{\mathbf{k}} + \text{c.c.})$. From this equation, we see only the real part of $\mathbf{e}^\dagger\mathbf{S}$ affects how the amplitude changes, while the imaginary part affects how the direction $\mathbf{e}$ rotates on the complex unit sphere.

The right-hand sides of the on-shell equations are originated from a single scattering term. As can be seen from identities (72) and (73), there exists some dimensionless scattering strength Θ^s, such that

$$\frac{e_s\omega_{ps}^2}{2m_sc}\frac{\varepsilon_1\varepsilon_2^*\varepsilon_3^*}{\omega_1\omega_2\omega_3}\Theta^s := -\frac{\mathcal{E}_1\cdot\mathbf{S}_{2,3}^*}{\omega_1^2} = \frac{\mathcal{E}_2^*\cdot\mathbf{S}_{1,\bar{3}}}{\omega_2^2} = \frac{\mathcal{E}_3^*\cdot\mathbf{S}_{1,\bar{2}}}{\omega_3^2}. \tag{77}$$

Using formula (71) for $\mathbf{S}_{2,3}$, we see that the normalized scattering strength can be written as the summation of strengths of six scattering channels

$$\Theta^s = \Theta^s_{1,\bar{2}\bar{3}} + \Theta^s_{\bar{2},\bar{3}1} + \Theta^s_{\bar{3},1\bar{2}} + \Theta^s_{1,\bar{3}\bar{2}} + \Theta^s_{\bar{2},1\bar{3}} + \Theta^s_{\bar{3},\bar{2}1}. \tag{78}$$

The normalized scattering strength due to each channel is given by the simple formula

$$\Theta^s_{i,jl} = \frac{1}{\omega_j}(c\mathbf{k}_i\cdot\mathbf{f}_{s,j})(\mathbf{e}_i\cdot\mathbf{f}_{s,l}), \tag{79}$$

where $\mathbf{f}_{s,j} := \mathbb{F}_{s,\mathbf{k}_j}\mathbf{e}_j$. In general, the normalized scattering strength $\Theta^s = \Theta^s_r + i\Theta^s_i$ contains both real and imaginary parts. In Sec. IV, we will show that the normalized scattering strength Θ^s is related to the reduced S matrix element of the quantized theory, and the six scattering channels correspond to the six ways of contracting a single interaction vertex.

Having expressed both the left- and the right-hand sides of the on-shell equations as scalars, we can now write the three-wave equations

$$d_ta_1 = -\frac{\Gamma}{\omega_1}a_2a_3, \tag{80}$$

$$d_ta_2 = \frac{\Gamma}{\omega_2}a_3a_1, \tag{81}$$

$$d_ta_3 = \frac{\Gamma}{\omega_3}a_1a_2, \tag{82}$$

where Γ is the coupling coefficient. Notice that due to the residual $\mathbb{Z}_2$ symmetry $a_j \to -a_j$, the sign of Γ is insignificant, as long as Eq. (80) has the opposite sign as Eqs. (81) and (82). Combining Eqs. (77)–(79), the coupling coefficient is given by

$$\Gamma = \sum_s\frac{Z_s\omega_{ps}^2\Theta_r^s}{4M_s(u_1u_2u_3)^{1/2}}, \tag{83}$$

where u_j is the wave energy coefficient, $Z_s := e_s/e$ and $M_s := m_s/m_e$ are the normalized charge and mass of species s, respectively. As expected, only the real part Θ_r^s of the normalized scattering strength affects the wave amplitude. Also notice when density $n_{s0} \to 0$, coupling due to species s vanishes as expected. The numerator of the coupling coefficient measures how strong the three waves are coupled by the scattering strength, and the denominator measures how energetically expensive to excite the linear waves, as measured by the wave energy coefficients.

It is instructive to count how many degrees of freedom the three-wave coupling coefficient Γ contains. For each wave, its 4-momentum is constrained by one dispersion relation. Once the 4-momentum is fixed, the wave polarization is determined by the dispersion tensor up to the wave amplitude, which Γ does not depend on. Therefore, for each wave, there are three degrees of freedom. Now that the resonant conditions give another four constrains, there are in total $3\times 3 - 4 = 5$ independent variables. Hence, in the absence of additional symmetry, the three-wave coupling coefficient Γ is a function of five independent variables in a given plasma.

Once the coupling coefficient is obtained in a given situation, the nonlinear three-wave equations (80)–(82) may

be solved using a number of techniques. For the homogeneous problem, where the spatial derivatives are zero, the equations become a system of nonlinear ordinary differential equations, and the general solutions are given by the Jacobi elliptic functions [37,38]. Similarly, in one dimension, the steady state problem, where the time derivatives are zero, can also be solved in terms of the Jacobi elliptic functions [39]. As a trivial extension, traveling wave solutions in one spatial dimension can also be found [40–42], using the coordinate transform $\xi = x - vt$. In addition to these periodic solutions, the nonlinear three-wave equations also have compact solutions, such as the N-soliton solutions [43,44]. More general solutions may also be constructed using the inverse scattering method [45,46]. In this paper, we will not be concerned with solving the three-wave equations, and only focus on calculating the coupling coefficient.

Without solving the three-wave equations, a number of experimental observables can already be extracted from the coupling coefficient. For example, Γ can be related to the growth rate of parametric instabilities. Consider the parametric decay instability where a pump wave with frequency ω_1 decays into two waves with frequencies ω_2 and ω_3. Suppose the pump has constant amplitude a_1, and the decay waves have no spatial variation. Then solving the linearized three-wave equations, we find a_2 and a_3 grow exponentially with rate

$$\gamma_0 = \frac{|\Gamma a_1|}{\sqrt{\omega_2 \omega_3}}. \tag{84}$$

The experimentally observed linear growth rate will be somewhat different than γ_0 due to wave damping. Wave damping, both collisional and collisionless, can be taken into account by inserting a phenomenological damping term νa into the left-hand side of the three-wave equations. Solving the linearized equations, the growth rate, modified by wave damping, is

$$\gamma = \sqrt{\gamma_0^2 + \left(\frac{\nu_2 - \nu_3}{2}\right)^2} - \frac{\nu_2 + \nu_3}{2}, \tag{85}$$

where ν_2 and ν_3 are the phenomenological damping rates of the two decay waves. In addition to wave damping, the experimentally observed growth rate can also be modified by frequency mismatch $\delta\omega = \omega_1 - \omega_2 - \omega_3$. When the frequency mismatch is much smaller than the spectral width of waves, the three waves can still couple almost resonantly. To find the growth rate in the presence of small $\delta\omega$, promote amplitude a to be complex and change variable $\alpha_j := a_j e^{-it\delta\omega/2}$ for $j = 2$ and 3. This change of variable is equivalent to modifying the damping rates to $\nu_2' := \nu_2 + i\delta\omega/2$ and $\nu_3'^* := \nu_3 - i\delta\omega/2$. Therefore, the growth rate of parametric decay instability, modified by both weak damping and small frequency mismatch, is

$$\gamma' = \sqrt{\gamma_0^2 + \left(\frac{\nu_2 - \nu_3 + i\delta\omega}{2}\right)^2} - \frac{\nu_2 + \nu_3}{2}. \tag{86}$$

The frequency mismatch $\delta\omega$ not only introduces amplitude modification, but also results in phase modification. In the following discussions, we shall only be concerned with the growth rate γ_0 as observable, ignoring wave damping and frequency mismatch.

IV. LAGRANGIAN OF THREE-WAVE INTERACTION

Now that we know how the coupling coefficient can be related to experimental observables, let us unveil why its formula looks the ways it is. Recall in the previous section, we show that the three-wave scattering strength $\mathbf{S}_{\mathbf{q},\mathbf{q}'}$ satisfies the action conservation laws. Motivated by these conservation laws, here in this section, we show that the three on-shell equations (65)–(67) can be derived from a classical three-wave Lagrangian. More importantly, we will show that all terms in the classical interaction Lagrangian arise from a single term after quantizing the Lagrangian.

To write the Lagrangian, it is more convenient to use the gauge field A^μ instead of the electric or magnetic fields. Since we will later quantize the Lagrangian, it is convenient to use the temporal gauge $A^0 = 0$. In temporal gauge, the electric field is related to the vector potential by

$$\mathbf{A}_\mathbf{k} = \frac{\mathcal{E}_\mathbf{k}}{\omega_\mathbf{k}}, \tag{87}$$

which, in the natural units $\hbar = c = 1$, has the dimension of energy M. Similarly, we can dimensionalize the wave energy operator $\mathbb{H}$ by

$$\Lambda_\mathbf{k} := \omega_\mathbf{k} \mathbb{H}_\mathbf{k}, \tag{88}$$

which then has the dimension of energy M as it should.

Having defined the necessary operators, we can now write the classical three-wave action for the three on-shell equations

$$S_c = \int d^4 x_{(1)} (\mathcal{L}_{c0} + \mathcal{L}_{cI}), \tag{89}$$

where the integrations over space and time are on the slow scales $x_{(1)}$ and $t_{(1)}$. Abbreviating the subscripts $\mathbf{k}_j$ as j, the Lagrangian of freely advecting wave envelopes

$$\mathcal{L}_{c0} = \sum_{j=1}^{3} \mathbf{A}_j^* \cdot i \Lambda_j d_{t(1)} \mathbf{A}_j, \tag{90}$$

where the complex amplitude $\mathbf{A}_j(x_{(1)}, t_{(1)})$ is a function of the slow spatial and temporal scales, and the advective derivative $d_{t(1)}$ is defined by Eq. (52). It is easy to show that $\mathcal{L}_{c0}$ gives rise to a real-valued action S_{c0} after integrating by parts. The second term in the classical action [Eq. (89)] is the three-wave interaction Lagrangian

$$\mathcal{L}_{cI} = -i(\Xi - \Xi^*), \tag{91}$$

which is obviously real valued. Using Eq. (77), the three waves interact through the coupling

$$\Xi = A_1 A_2^* A_3^* \sum_s \frac{e_s \omega_{ps}^2}{2 m_s c} \Theta^s, \tag{92}$$

where Θ^s is the normalized scattering strength [Eq. (78)], and the A's are the scalar amplitudes of the three waves. Clearly, the coupling Ξ has mass dimension M^4, and hence the action S_{cI} is dimensionless in the natural unit as expected. Now that we have written the Lagrangian, we can find the classical equations of motion by taking variations with respect to $\mathbf{A}_1$, $\mathbf{A}_2$, and $\mathbf{A}_3$ or, equivalently, their independent complex conjugates. Using the self-adjointness [Eq. (29)] of the forcing operator,

it is straightforward to verify that the three on-shell equations (65)–(67) are the resultant equations.

The classical three-wave Lagrangian $\mathcal{L}_c = \mathcal{L}_{c0} + \mathcal{L}_{cI}$ has U(1) symmetries, which lead to the action conservation laws. For example, the Lagrangian is invariant under the following global U(1) transformation

$$\mathbf{A}_1 \to e^{i\alpha}\mathbf{A}_1, \tag{93}$$

$$\mathbf{A}_2 \to e^{i\alpha}\mathbf{A}_2, \tag{94}$$

$$\mathbf{A}_3 \to \mathbf{A}_3, \tag{95}$$

where α is an arbitrary real constant. Under the above transformation, the infinitesimal variation of the Lagrangian is zero $\delta\mathcal{L}_c = 0$, while the infinitesimal variation $\delta\mathbf{A}_1 = i\alpha\mathbf{A}_1$, $\delta\mathbf{A}_2 = i\alpha\mathbf{A}_2$, and $\delta\mathbf{A}_3 = 0$, giving rise to a Noether's current. In fact, we have an even stronger symmetry $\delta\Xi = 0$ for any α. Therefore, this U(1) symmetry leads to the identity

$$\mathbf{A}_1 \cdot \frac{\delta\Xi}{\delta\mathbf{A}_1} - \mathbf{A}_2^* \cdot \frac{\delta\Xi}{\delta\mathbf{A}_2^*} = 0, \tag{96}$$

which is exactly the action conservation law (72). Using similar arguments, other action conservation laws can be derived from other global U(1) symmetries.

The large number of terms contained in the classical Lagrangian can be reduced when we quantized the Lagrangian, in which the gauge field becomes real valued. Before introducing the quantized Lagrangian, it is helpful to review the second quantization notations. For simplicity, we will omit the subscripts for the slow spatial and temporal variables $x_{(1)}$ and $t_{(1)}$, with the implied understanding that all spatial and temporal dependencies are on the full scales. Let us promote the gauge field $\mathbf{A}$ to quantized operator

$$\hat{\mathbf{A}} := \int \frac{d^3\mathbf{k}}{(2\pi)^3}\frac{1}{\sqrt{2\omega_\mathbf{k}}}(\mathbf{e}_\mathbf{k}\hat{a}_\mathbf{k}e^{-ikx} + \mathbf{e}_\mathbf{k}^*\hat{a}_\mathbf{k}^\dagger e^{ikx}), \tag{97}$$

where $kx := \omega_\mathbf{k}t - \mathbf{k}\cdot\mathbf{x}$ is the Minkowski inner product, $\mathbf{e}_\mathbf{k}$ is the unit polarization vector, and the summation over branches of the dispersion relation is implied. The annihilation operator $\hat{a}_\mathbf{k}$ and the creation operator $\hat{a}_\mathbf{k}^\dagger$ satisfy the canonical commutation relations for bosons, where the nontrivial commutator is

$$[\hat{a}_\mathbf{p}, \hat{a}_\mathbf{k}^\dagger] = (2\pi)^3\delta^{(3)}(\mathbf{p}-\mathbf{k}). \tag{98}$$

Using the standard normalization, the single boson state

$$|\mathbf{k}\rangle := \sqrt{2\omega_\mathbf{k}}\hat{a}_\mathbf{k}^\dagger|0\rangle, \tag{99}$$

where $|0\rangle$ is the vacuum state. Then, we have the following Wick contraction:

$$\hat{\mathbf{A}}|\mathbf{k}\rangle = \mathbf{e}_\mathbf{k}e^{-ikx}. \tag{100}$$

Let us also promote the displacement operator for species s to act on the operator $\hat{\mathbf{A}}$ by

$$\hat{\Pi}_s\hat{\mathbf{A}} := i\int \frac{d^3\mathbf{k}}{(2\pi)^3}\frac{1}{\sqrt{2\omega_\mathbf{k}}}\left(\frac{\mathbb{F}_{s,\mathbf{k}}\mathbf{e}_\mathbf{k}}{\omega_\mathbf{k}}\hat{a}_\mathbf{k}e^{-ikx} - \frac{\mathbb{F}_{s,\mathbf{k}}^*\mathbf{e}_\mathbf{k}^*}{\omega_\mathbf{k}}\hat{a}_\mathbf{k}^\dagger e^{ikx}\right), \tag{101}$$

where the minus sign in front of the second term comes from notation (22). Taking time derivative of the displacement operator, $\partial_t(\hat{\Pi}_s\hat{\mathbf{A}})$ is the velocity operator for species s, which is proportional to the current operator.

Now, we are ready to write the quantized Lagrangian, which contains a kinetic term and a single three-wave coupling term:

$$\mathcal{L} = \hat{\mathbf{A}}^\dagger i\Lambda d_t\hat{\mathbf{A}} - \sum_s \frac{e_s\omega_{ps}^2}{2m_s}(\hat{\Pi}_s\hat{\mathbf{A}})_i(\partial_i\hat{\mathbf{A}}_j)\partial_t(\hat{\Pi}_s\hat{\mathbf{A}})_j. \tag{102}$$

Here, the i and j indices in the second term are the spatial indices, and summation over repeated indices is assumed. The first term $\mathcal{L}_0$ closely resembles the kinetic term of quantum electrodynamics (QED), with the Dirac spinor replaced by the gauge field, and the Dirac gamma matrices replaced by the Λ energy matrix. The second term $\mathcal{L}_I$ is the three-wave interaction Lagrangian, which is nonvanishing only if the background density of some species s is nonzero. Notice that the three-wave interaction is nonrenormalizable, which is not unexpected in an effective field theory.

To make sense of the quantized Lagrangian, we recognize that the displacement $\hat{\Pi}_s\hat{\mathbf{A}}$ is proportional to the polarization density $\mathbf{P}$, and the velocity $\partial_t(\hat{\Pi}_s\hat{\mathbf{A}})$ is proportional to the current density $\mathbf{J}$. Therefore, the three-wave interaction Lagrangian is of the form $\mathcal{L}_I \propto P^i(\partial_i\mathbf{A}_j)J^j$, where the polarization and current density are determined by linear response. Although one may not have guessed this form of the interaction Lagrangian, it makes the following intuitive sense: in the absence of the third wave, the electromagnetic field interacts with the particle fields through $\mathbf{A}_j J^j$ in the temporal gauge; now, when the third wave is present, it modulates the medium through which the electromagnetic field advects, giving rise to the $P^i(\partial_i\mathbf{A}_j)J^j$ interaction. In this interaction term, there is no reason why a particular wave should only be responsible for $\mathbf{P}$, $\mathbf{A}$, or $\mathbf{J}$. Therefore, the three waves can switch their roles, and the total interaction is given by linear superpositions of all possible permutations.

To see how the quantized Lagrangian, with the linear superposition principle built in, gives rise to the classical Lagrangian, let us compute the S matrix element of three-wave decay $\mathbf{k}_1 \to \mathbf{k}_2 + \mathbf{k}_3$. The S matrix element

$$\langle\mathbf{k}_2,\mathbf{k}_3|i\mathcal{L}_I|\mathbf{k}_1\rangle = i\mathcal{M}e^{i(k_2+k_3-k_1)x}, \tag{103}$$

where the reduced matrix element $i\mathcal{M}$ can be represented using Feynman diagrams

$i\mathcal{M} =$ 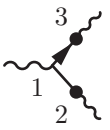 $+ 5$ permutations. (104)

Since there are three external boson lines, each connecting to one of the three vertices, there are in total $3! = 6$ Feynman diagrams. In the above Feynman diagram, interaction vertex to which 1 is connected to is the usual QED vertex, whereas vertices 2 and 3 appear only when there are background particle fields [47]. The arrow between vertices 1 and 3 indicates the direction of momentum flow, and also labels which vertex the ∂_t derivative acts on. The above Feynman diagram corresponds

to the particular Wick contraction

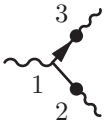

$$= -i\frac{e_s\omega_{ps}^2}{2m_s}\langle \mathbf{k}_2, \mathbf{k}_3|(\hat{\Pi}_s\hat{\mathbf{A}})_j(\partial_j\hat{\mathbf{A}}_l)\partial_t(\hat{\Pi}_s\hat{\mathbf{A}})_l|\mathbf{k}_1\rangle$$

$$= i\frac{e_s\omega_{ps}^2}{2m_sc}\Theta^s_{1,2\bar{3}}. \tag{105}$$

Summing with the other five Feynman diagrams, the reduced S matrix element in the quantum theory is related to the normalized scattering strength in the classical theory by the simple relation

$$\mathcal{M} = \sum_s \frac{e_s\omega_{ps}^2}{2m_sc}\Theta^s. \tag{106}$$

From the Lagrangian perspective, the classical three-wave coupling is related to the quantized interaction through the S matrix

$$i\,\Xi = A_1A_2^*A_3^*\langle \mathbf{k}_2,\mathbf{k}_3|i\mathcal{L}_I|\mathbf{k}_1\rangle e^{i(k_1-k_2-k_3)x}. \tag{107}$$

Using the above relation, we immediately recover the classical three-wave coupling by computing the S matrix element using the quantized Lagrangian. Alternatively, one may simply regard Lagrangian (102) as a classical Lagrangian, and substitute Eq. (97) as the spectral expansion of the gauge field. Then, after integrating over spacetime, $\int d^4x\ \exp[i(k_1-k_2-k_3)x] = (2\pi)^4\delta^{(4)}(k_1-k_2-k_3)$ will select out the six resonate terms from the interaction Lagrangian.

Now that we understand how the classical theory and the quantized theory are connected, we may postulate that the three-wave coupling always arises from the $P^i(\partial_i\mathbf{A}_j)J^j$ term in the effective Lagrangian, regardless of the plasma model that is used to calculate the linear response. In the cold fluid model, the linear response is expressed in terms of the forcing operator $\mathbb{F}$. By modifying this operator to include thermal or even quantum effects, and plugging it into the formalism we have developed, the three-wave scattering strength may be evaluated immediately. Having obtained the normalized scattering strength, as well as the wave energy coefficients in that particular plasma model, one can then compute the three-wave coupling coefficient using Eq. (83). We have thus conjectured a prescription for computing three-wave coupling, without the need for going through the perturbative solution of the equations. The coupling coefficient then enters the three-wave equation, which governs the evolution of the envelopes of the three waves.

V. SCATTERING OF QUASITRANSVERSE AND QUASILONGITUDINAL WAVES

In this section, we use two sets of examples to demonstrate how to evaluate the three-wave coupling coefficient. The coupling coefficient (83) can be readily evaluated in cold fluid model using wave energy coefficient (75) and normalized scattering strength (79). When using these formulas in the most general geometry (Fig. 1), we need to ensure that the resonant conditions (61) and (62) are satisfied by three otherwise arbitrary "on-shell" waves. The evaluation becomes particularly easy when waves are either quasitransverse (T) or quasilongitudinal (L). In these situations, the wave dispersion relations are simplified, and hence matching resonance conditions becomes an easy task. Moreover, for both T and L waves, the wave polarization vectors are at special angles with the wave vector, so that the expressions for the wave energy and scattering strength can be further simplified. Although T and L waves can couple with other waves that have both electrostatic and electromagnetic components, we will only give examples where all three participating waves are either T or L waves.

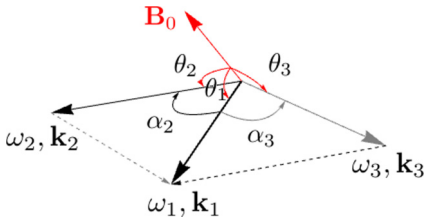

FIG. 1. The most general geometry of three-wave scattering in a uniform plasma with a constant magnetic field. The three wave vectors $\mathbf{k}_1 = \mathbf{k}_2 + \mathbf{k}_3$ are in the same plane, and are at angles θ with respect to the magnetic field.

In general, there are four different three-wave triplets: $\{T,T,T\}$, $\{T,T,L\}$, $\{T,L,L\}$, and $\{L,L,L\}$. However, only two of these triplets can couple resonantly. From Appendix B, we know the T waves are electromagnetic waves with $\omega \gg \omega_p, |\Omega_e|$, while the L waves are electrostatic waves with $\omega \to \omega_r$, for some resonance $\omega_r \sim \omega_p, |\Omega_e|$. Since the frequency of a T wave is much higher than the frequency of an L wave, only the following two types of interactions can match frequency resonance:

$$T \rightleftharpoons T + L, \tag{108}$$

$$L \rightleftharpoons L + L. \tag{109}$$

A typical scenario for the *TTL* interaction is the scattering of lasers. For example, an incident laser is scattered inelastically by some plasma waves and thereafter propagates in some other direction with shifted frequency. Similarly, a typical scenario for the *LLL* interaction is the decay of a plasma wave launched by some antenna array. In what follows, we will consider these two scenarios in detail. We will first reproduce well-known results for collimated *TTL* interaction, and then present previously unknown results in more general geometry.

A. $T \rightleftharpoons T + L$ scattering

Consider the decay of a pump laser (ω_1) into a scattered laser (ω_2) and a plasma wave (ω_3). Since the frequency $\omega_{1,2} \gg \Omega_s$, the magnetization ratio $\beta_{1,2} \simeq 0$ and the magnetization factor $\gamma_{1,2} \simeq 1$ for any species. Consequently, the forcing operator $\mathbb{F}_{1,2} \simeq \mathbb{I}$ is approximately the identity operator, and the lasers are therefore transverse electromagnetic waves. As for the plasma wave, using the quasilongitudinal approximation $\mathbf{e}_3 \simeq \hat{\mathbf{k}}_3$, the inner products are purely real:

$$\hat{\mathbf{k}}_3 \cdot \hat{\mathbf{f}}^*_{s,3} \simeq \hat{\mathbf{k}}_3 \cdot \mathbb{F}_{s,3}\hat{\mathbf{k}}_3 = \gamma^2_{s,3}\big(1 - \beta^2_{s,3}\cos^2\theta_3\big), \tag{110}$$

where θ_3 is the angle between $\mathbf{k}_3$ and $\mathbf{b}$ as shown in Fig. 1, and $\hat{\mathbf{k}}_3$ is the unit vector along $\mathbf{k}_3$ direction. With this basic setup, we can readily evaluate Eq. (83), the coupling coefficient.

Let us first calculate the wave energy coefficients (75), which enter the denominator of the coupling coefficient. Since $\mathbb{F}_{1,2} \simeq \mathbb{I}$, the wave energy coefficients for the lasers are simply

$$u_1 \simeq u_2 \simeq 1. \tag{111}$$

As for the plasma wave, after taking the frequency derivative in Eq. (36), the wave energy coefficient for quasilongitudinal wave is

$$u_3 \simeq 1 + \sum_s \frac{\omega_{ps}^2}{\omega_3^2} \gamma_{s,3}^4 \beta_{s,3}^2 \sin^2\theta_3. \tag{112}$$

As expected, u_3 is always positive, although $\gamma_{s,3}^2$ can be either positive or negative, depending on whether $\beta_{s,3}$ is either smaller or larger than one.

To find the normalized scattering strength (78), which enters the numerator of Γ, we again use the fact $\omega_{1,2} \gg \omega_3$. Since the wave vectors are comparable in magnitudes, the dominant terms of the coupling strength are the two terms proportional to $1/\omega_3$, if the inner product $\mathbf{e}_1 \cdot \mathbf{f}_2^* \simeq \mathbf{f}_1 \cdot \mathbf{e}_2^* \simeq \mathbf{e}_1 \cdot \mathbf{e}_2^*$ is of order unity. Using the resonance condition $\mathbf{k}_1 - \mathbf{k}_2 = \mathbf{k}_3$, the dominant term of the *TTL* scattering strength

$$\Theta^s \simeq -\frac{ck_3}{\omega_3} (\hat{\mathbf{k}}_3 \cdot \mathbb{F}_{s,3} \hat{\mathbf{k}}_3)(\mathbf{e}_1 \cdot \mathbf{e}_2^*), \tag{113}$$

where the inner product $\hat{\mathbf{k}}_3 \cdot \mathbb{F}_{s,3} \hat{\mathbf{k}}_3$ is given explicitly by Eq. (110). Now that we have simplified both the denominator and the numerator of Eq. (83), a simple formula for the three-wave coupling coefficient Γ can be obtained.

Having obtained an explicit formula for the coupling coefficient, we can use it to obtain expressions for experimental observables. For example, the linear growth rate γ_0 [Eq. (84)] can be decomposed as

$$\gamma_0 = \gamma_R |\mathcal{M}_T|, \tag{114}$$

where γ_R is the backward Raman growth rate when the plasma is unmagnetized,

$$\gamma_R = \frac{\sqrt{\omega_1 \omega_p}}{2} |a_1 \mathrm{Re}(\mathbf{e}_1^* \cdot \mathbf{e}_2)|, \tag{115}$$

and $\mathcal{M}_T$ is the normalized growth rate of the *TTL* scattering. The normalized growth rate is proportional to the coupling coefficient $\Gamma = \omega_p^2 \mu / 4$ up to some kinematic factor

$$\mathcal{M}_T = \frac{1}{2} \left(\frac{\omega_p^3}{\omega_1 \omega_2 \omega_3} \right)^{1/2} \mu_T, \tag{116}$$

where the normalized coupling coefficient μ_T is given by

$$\mu_T \simeq \sum_s \frac{Z_s}{M_s} \frac{\omega_{ps}^2}{\omega_p^2} \frac{ck_3}{\omega_3} \frac{\hat{\mathbf{k}}_3 \cdot \mathbb{F}_{s,3} \hat{\mathbf{k}}_3}{u_3^{1/2}} \tag{117}$$

in the *TTL* approximation. In the unmagnetized limit $B_0 \to 0$, we have $\beta_3 \to 0$ and $\gamma_3 \to 1$. Since ion mass is much larger than electron mass, we have $\mu_T \to -ck_3/\omega_3$. Moreover, since the lasers can only couple through the Langmuir wave in cold unmagnetized plasma, we have $\omega_3 \to \omega_p$. Then, the normalized growth rate $\mathcal{M}_T \to ck_3/2\sqrt{\omega_1 \omega_2}$. Finally, in backward scattering geometry $ck_3 = ck_1 + ck_2 \simeq \omega_1 + \omega_2 \simeq 2\omega_0$, where we have denoted $\omega_0 := \omega_1 \simeq \omega_2$. We see $\mathcal{M}_T \to 1$ in the unmagnetized limit as expected.

The normalized growth rate becomes particularly simple when waves propagate at special angles. For example, consider the situation where the three waves propagate along the magnetic field $\mathbf{B}_0$, and the plasma wave $\omega_3 = \omega_p$ is the Langmuir wave. Since $\gamma_{s,3}^2$ remains finite as $\theta_3 \to 0$, the normalized growth rate for collimated parallel wave propagation is

$$\mathcal{M}_{T\parallel}^P \simeq -\frac{1}{2} \frac{ck_3}{\sqrt{\omega_1 \omega_2}}, \tag{118}$$

where we have used $M_i \gg 1$ to drop the summation over species. The above is exactly the same as the unmagnetized result [12,23], which is expected because the plasma wave is not affected by the parallel magnetic field.

To give another simple example, consider the situation where the three waves are collimated and propagate perpendicular to the magnetic field $\mathbf{B}_0$. In cold electron-ion plasma, there are two L waves in the perpendicular direction: the upper-hybrid (*UH*) wave and the lower-hybrid (*LH*) wave. Let us first consider scattering mediated by the *UH* wave $\omega_3 \simeq \omega_{UH} \simeq \sqrt{\omega_p^2 + \Omega_e^2}$. In this situation, the magnetization factor $\gamma_{3,e}^2 \simeq \omega_{UH}^2/\omega_p^2$ and $\gamma_{3,i}^2 \simeq 1$. Since $M_i \gg 1$, the dominant contribution for both the wave energy coefficient and the scattering strength comes from electrons. The wave energy coefficient $u_3 \simeq \omega_{UH}^2/\omega_p^2$, and the normalized coupling coefficient $\mu_T \simeq -ck_3/\omega_p$. Therefore, the normalized growth rate for collimated perpendicular wave propagation mediated by the *UH* wave is

$$\mathcal{M}_{T\perp}^{UH} \simeq -\frac{1}{2} \frac{ck_3}{\sqrt{\omega_1 \omega_2}} \left(\frac{\omega_p}{\omega_{UH}} \right)^{1/2}. \tag{119}$$

Similarly, let us consider scattering mediated by the *LH* wave $\omega_3 \simeq \omega_{LH} \simeq \sqrt{|\Omega_e| \Omega_i} \omega_p / \omega_{UH}$. Since the *LH* frequency satisfies $\Omega_i \ll \omega_{LH} \ll |\Omega_e|$, the magnetization ratios $\beta_{3,e} \gg 1$ and $\beta_{3,i} \ll 1$. Consequently, the magnetization factor $\gamma_{3,e} \simeq -1/\beta_{3,e}^2$ and $\gamma_{3,i} \simeq 1$. When $\omega_p \sim |\Omega_e|$ are comparable, electron contributions again dominate. The wave energy coefficient $u_3 \simeq \omega_{UH}^2/\Omega_e^2$, and the normalized coupling coefficient $\mu_T \simeq ck_3 \omega_{LH}/\omega_{UH}|\Omega_e|$. Therefore, the normalized growth rate for *LH* wave mediation in the collimated perpendicular geometry is

$$\mathcal{M}_{T\perp}^{LH} \simeq \frac{1}{2} \frac{ck_3}{\sqrt{\omega_1 \omega_2}} \frac{\omega_p^{3/2} \omega_{LH}^{1/2}}{\omega_{UH} |\Omega_e|}. \tag{120}$$

The above examples recover results known in Ref. [19], who analyze the same problem in the restricted geometry where the the waves are collimated and propagate perpendicular to the magnetic field.

Having reproduced well-known results, let us evaluate the normalized growth rate in more general geometry, where the waves are not collimated and propagate at angles with respect to the magnetic field. The normalized growth rate can be evaluated using the following procedure, mimicking what happens in an actual experiment where the plasma density and magnetic field strength are known. First, we shine a laser with frequency ω_1 into the plasma at some angle θ_1 with respect to the magnetic field. Then, the wave vector k_1 is known from the dispersion relation. Second, we observe the scattered laser using some detector placed at angle θ_2 with respect to the magnetic field, and point

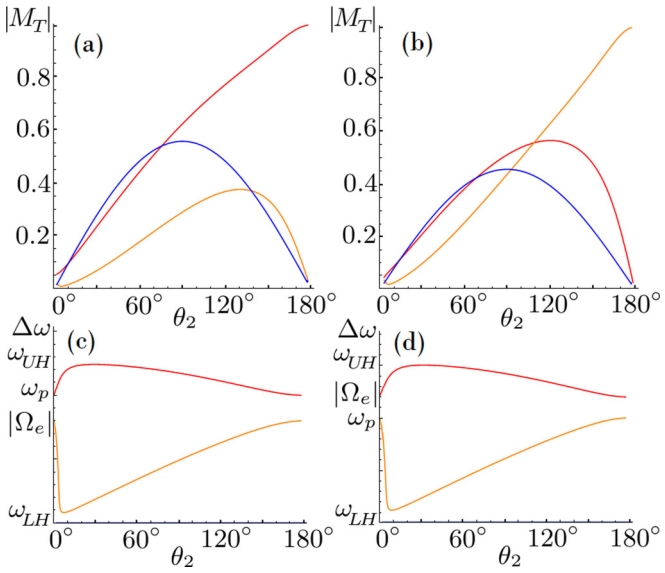

FIG. 2. Scattering of a parallel pump laser in uniform hydrogen plasmas. The pump laser has frequency $\omega_1/\omega_p = 10$, and the scattered laser propagates at angle θ_2 with respect to $\mathbf{k}_1 \| \mathbf{B}_0$. The laser can scatter from the upper resonance (red), the lower resonance (orange), and the bottom resonance (blue). When the plasma is overdense, e.g., $|\Omega_e|/\omega_p = 0.8$ (a), (c), the upper resonance is of Langmuir type, while the lower and bottom resonances are cyclotronlike; when the plasma is underdense, e.g., $|\Omega_e|/\omega_p = 1.2$ (b), (d), the lower resonance is of Langmuir type, while the upper and bottom resonances are cyclotronlike. For Langmuir-type resonance, the frequency shift (c), (d) $\Delta\omega \to \omega_p$, and the normalized growth rate (a), (b) is monotonously increasing; while for cyclotronlike resonances, $\Delta\omega \to |\Omega_e|, \Omega_i$, and the normalized growth rate $|\mathcal{M}_T|$ peaks at intermediate θ_2, while becoming zero for exact backscattering. See text for how $|\mathcal{M}_T|$ scales with plasma parameters.

the detector at angle α_2 with respect to the incoming laser. Suppose the detector can measure the frequency ω_2 of the scattered laser, then from this frequency information, we immediately know k_2 from the dispersion relation, as well as $\omega_3 = \omega_1 - \omega_2$ from the resonance condition. Next, we can calculate $k_3 = \sqrt{k_1^2 + k_2^2 - 2k_1k_2\cos\alpha_2}$, and determine θ_3 by inverting $\omega_3 = \omega_r(\theta_3)$, where ω_r is the angle-dependent resonance frequency. Using this procedure, the normalized growth rate can be readily evaluated numerically. Conversely, when plasma density and magnetic field are unknown, we may use information measured from laser scattering experiments to fit plasma parameters.

1. Parallel pump

To demonstrate how to evaluate the normalized growth rate $\mathcal{M}_T$, consider the example where the incident laser propagates along the magnetic field, while the scattered laser propagates at some angle θ_2. In this case $\alpha_2 = \theta_2$, and by cylindrical symmetry, $\mathcal{M}_T$ depends on only one free parameter θ_2, as plotted in Fig. 2 for hydrogen plasma with $\omega_1/\omega_p = 10$. When there are only two charged species, as in the case of hydrogen plasma, there are three electrostatic resonances the lasers can scatter from (Fig. 8). The first resonance is the upper resonance, whose frequency asymptotes to the upper-hybrid frequency ω_{UH} when $\theta_3 \to \pi/2$. When scattered from the upper resonance (red curves), the scattered laser is frequency down-shifted ($\Delta\omega = \omega_1 - \omega_2$) by the largest amount. The second resonance is the lower resonance, whose frequency asymptotes to the lower-hybrid frequency ω_{LH} when $\theta_3 \to \pi/2$. When scattered from the lower resonance (orange curves), the scattered laser is frequency shifted by either $|\Omega_e|$ in overdense plasma ($|\Omega_e| < \omega_p$) or by ω_p in underdense plasma ($|\Omega_e| > \omega_p$), when $\theta_3 \to 0$. The third resonance is the bottom resonance, whose frequency asymptotes to 0 when $\theta_3 \to \pi/2$. When scattered from the bottom resonance (blue curves), the scattered laser is frequency shifted by at most Ω_i when $\theta_3 \to 0$. Since Ω_i is much smaller than other frequency scales, the frequency shift $\Delta\omega$ for scattering off the bottom resonance is not discernible in Figs. 2(c) and 2(d). In terms of the normalized growth rate (upper panels), we see $\mathcal{M}_T \to 1$ when the laser is backscattered from the Langmuir resonance with $\Delta\omega \to \omega_p$, while $\mathcal{M}_T \to 0$ when the laser is scattered from the cyclotron resonances with $\Delta\omega \to |\Omega_e|, \Omega_i$. For Langmuir-type resonance, $\mathcal{M}_T$ increases monotonously with θ_2. In contrast, for cyclotronlike resonances, $\mathcal{M}_T$ peaks at intermediate θ_2, and becomes zero for exact backscattering.

To better understand the angular dependence of the normalized growth rate $\mathcal{M}_T$, let us find its asymptotic expressions. In the limit $\omega_{1,2} \gg \omega_3$, the wave vector $k_2/k_1 \simeq 1$ and $k_3/k_1 \simeq 2\sin(\theta_2/2)$. At finite angle $\theta_2 > 0$, we can approximate $\theta_3 \simeq (\pi - \theta_2)/2$. For even larger θ_2, we can also approximate the resonance frequency ω_3 using Eqs. (B11)–(B13) because $\theta_3 \sim 0$ is now small. These asymptotic geometric relations will be useful when we evaluate the coupling coefficient.

First, consider scattering off the Langmuir-type resonance $\omega_3 \sim \omega_p$. Since $\gamma_{3,s}$ is finite, the lowest order angular dependence comes from k_3. Take the limit $\theta_3 \to 0$, we get Eq. (118). Now, retain the angular dependence of k_3, we can grossly approximate

$$|\mathcal{M}_T^p| \simeq \sin\frac{\theta_2}{2}. \tag{121}$$

This approximation is of course very crude, but it captures the monotonous increasing feature for scattering off the Langmuir-type resonance. In fact, the above result becomes a very good approximation when the magnetic field $B_0 \to 0$. In this unmagnetized limit, we recover the angular dependence of Raman scattering.

Second, consider scattering off the electron-cyclotron-like resonance $\omega_3 \sim |\Omega_e|$. Notice that in this case, the magnetization factor $\gamma_{3,e}^2 \gg 1$ for small θ_3. Nevertheless, since both the numerator and the denominator contain this factor, $\mathcal{M}_T$ remains finite. For electrons, the magnetization ratio $\beta_{3,e} \simeq 1$. Using Eq. (B12), which is valid when $\omega_p \neq |\Omega_e|$, the magnetization factor $\gamma_{3,e}^2 \simeq (\Omega_e^2 - \omega_p^2)/(\omega_p^2\sin^2\theta_3)$. In comparison, $\beta_{3,i} \ll 1$ and $\gamma_{3,i}^2 \simeq 1$. Hence, the dominant contribution comes from electrons. Substituting these into Eq. (116), we see to leading order

$$|\mathcal{M}_T^e| \simeq \frac{1}{2}\left(\frac{\omega_p}{\omega_3}\right)^{1/2}\sin\theta_2, \tag{122}$$

where ω_3 as function of θ_2 is given by Eq. (B12), with $\theta_3 \simeq (\pi - \theta_2)/2$. From Eq. (122), we see $|\mathcal{M}_T^e|$ reaches maximum when the laser is scattered almost perpendicularly to the magnetic field. The maximum value scales roughly as $|\mathcal{M}_T^e| \sim \sqrt{\omega_p/|\Omega_e|}/2$, which can be very large in weakly magnetized plasmas, as long as the cold fluid approximation remains valid. Away from $\theta_2 \sim \pi/2$, the normalized growth rate $|\mathcal{M}_T^e|$ falls off to zero. This falloff is expected because exciting cyclotron resonance is energetically forbidden.

In the end, consider scattering off ion-cyclotron-like resonance $\omega_3 \sim \Omega_i$. In this case, the ion contribution to the wave energy coefficient is no longer negligible because $\beta_{3,i} \simeq 1$ and $\gamma_{3,i}^2 \simeq \Omega_e/\Omega_i \tan^2(\theta_2/2) \gg 1$, as can be seen from Eq. (B13). The scattering strength is still dominated by electrons, for which $\beta_{3,e} \gg 1$, and $\gamma_{3,e}^2 \simeq -1/\beta_{3,e}^2 \ll 1$. Substituting these into Eq. (116), the normalized growth rate

$$|\mathcal{M}_T^i| \simeq \frac{1}{2}\left(\frac{\omega_p\,\Omega_i}{|\Omega_e|\omega_3}\right)^{1/2} \sin\theta_2. \tag{123}$$

We see the above result is rather similar to Eq. (122), except that $\omega_3 \sim \Omega_i$ has very weak angular dependence. Therefore, $|\mathcal{M}_T^i|$ is very well approximated by Eq. (123). The normalized growth rate peaks almost at $\theta_2 = \pi/2$, reaching a maximum $|\mathcal{M}_T^i| \sim \sqrt{\omega_p/|\Omega_e|}/2$, which can be very large in weakly magnetized plasmas. Similar to the electron cyclotron case, $|\mathcal{M}_T^i|$ falls off to zero for parallel scattering.

2. *Perpendicular pump*

Consider the other special case where the pump laser propagates perpendicular to the magnetic field. In this geometry, it is natural to plot the normalized growth rate $|\mathcal{M}_T|$ in spherical coordinate (Fig. 3), where the polar angle θ_2 is measured from the magnetic field $\mathbf{B}_0$, and the azimuthal angle ϕ_2 is measured from the wave vector $\mathbf{k}_1$. By symmetry of this setup, it is obvious that $\mathcal{M}_T(\phi_2,\theta_2) = \mathcal{M}_T(\phi_2,\pi - \theta_2) = \mathcal{M}_T(-\phi_2,\theta_2)$. Therefore, it is sufficient to consider the range $\theta_2 \in [0,\pi/2]$ and $\phi_2 \in [0,\pi]$. By matching the $\mathbf{k}$ resonance, we can read θ_3 from the spherical coordinates (ϕ_2,θ_2), and thereafter read the frequency shift ω_3 from Fig. 8. As for the growth rate, in electron-ion plasma, when scattered from the upper resonance [Fig. 3(a)], backscattering has the largest growth rate. While for scattering off the lower resonance [Fig. 3(b)], $|\mathcal{M}_T|$ reaches maximum for both backscattering and nearly parallel scattering, where the scattered laser propagates almost parallel to the magnetic field. In comparison, when scattering off the bottom resonance [Fig. 3(c)], the normalized growth rate peaks for nearly backward scattering, while it falls to zero for exact backscattering.

To better understand the angular dependence of the normalized growth rate, let us consider its asymptotic expressions for two special cases. The first special case is when all waves lie in the plane perpendicular to the magnetic field, namely, when $\theta_2 = 90^\circ$. In this case, the angle θ_3 is fixed to 90°, and the frequency of the plasma resonances are also fixed to ω_{UH}, ω_{LH}, or zero. Therefore, the angular dependence only comes from k_3. In the limit $\omega_{1,2} \gg \omega_3$, we have $k_3 \simeq 2k_1 \sin(\phi_2/2)$. Using Eqs. (119) and (120), it is easy to see, for scattering off

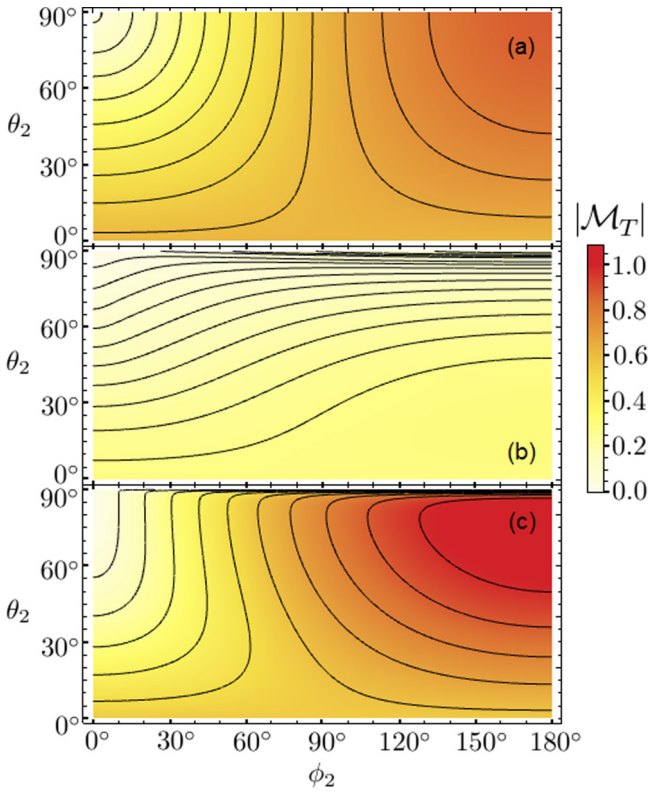

FIG. 3. Normalized growth rate $|\mathcal{M}_T|$ for scattering of a perpendicular pump laser ($\mathbf{k}_1 \perp \mathbf{B}_0$) in a uniform hydrogen plasma with $\omega_1/\omega_p = 10$ and $|\Omega_e|/\omega_p = 0.8$. In spherical coordinate, the scattered laser propagates at polar angle θ_2 with respect to $\mathbf{B}_0$, and azimuthal angle ϕ_2 measured from $\mathbf{k}_1$. The laser can scatter from the upper resonance (a), in which case backscattering is the strongest scattering mode. Alternatively, the laser can scatter off the lower resonance (b). In this case, one maximum of $|\mathcal{M}_T|$ is attained for backscattering, and another maximum is attained when the scattered laser propagates almost perpendicular to the incident laser along the magnetic field. Finally, the laser can scatter off the bottom resonance (c). In this case, exact backscattering is suppressed while nearly backward scattering is strong.

UH and *LH* waves in the perpendicular plane

$$|\mathcal{M}_{T\perp}^{UH}| \simeq \left(\frac{\omega_p}{\omega_{UH}}\right)^{1/2} \sin\frac{\phi_2}{2}, \tag{124}$$

$$|\mathcal{M}_{T\perp}^{LH}| \simeq \frac{\omega_p^{3/2}\omega_{LH}^{1/2}}{\omega_{UH}|\Omega_e|} \sin\frac{\phi_2}{2}. \tag{125}$$

Now, let us calculate $\mathcal{M}_{T\perp}^b$ for scattering off the bottom resonance. Using asymptotic expression (B16) for ω_3, we see although the magnetization ratio $\beta_{3,s} \to \infty$, the product $\beta_{3,s}\cos\theta_3$ remains finite as $\theta_3 \to \pi/2$. Since the magnetization factor $\gamma_{3,s} \simeq -1/\beta_{3,s}^2 \ll 1$, it is easy to see $\mathcal{M}_{T\perp}^b \propto \sqrt{\omega_3}$, which goes to zero when $\theta_3 \to \pi/2$. Hence, for scattering off the bottom resonance in the perpendicular plane

$$|\mathcal{M}_{T\perp}^b| = 0 \tag{126}$$

is completely suppressed. Consequently, exact backscattering from the bottom resonance is also suppressed.

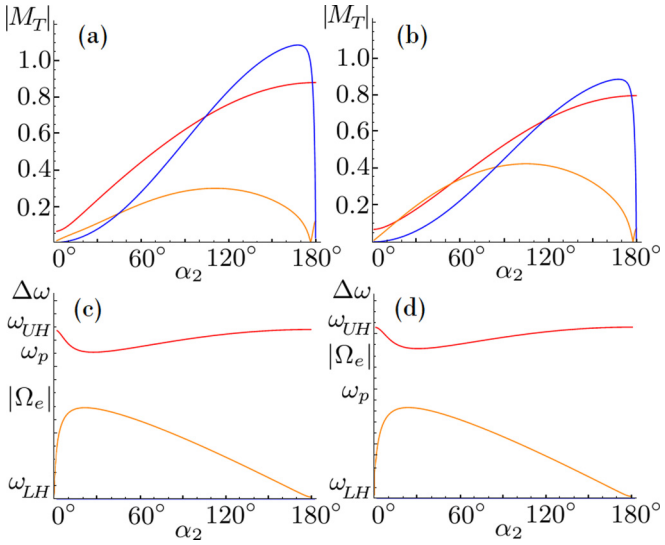

FIG. 4. Scattering of a perpendicular pump laser with $\omega_1/\omega_p = 10$ in a uniform hydrogen plasma. Figure (a) can be obtained from Fig. 3 by taking a one dimensional cut along the unit sphere using the plane spanned by $\mathbf{k}_1 \perp \mathbf{B}_0$. The scattered laser, propagating at angle α_2 with respect to $\mathbf{k}_1$, can scatter from the upper resonance (red), the lower resonance (orange), and the bottom resonance (blue). Both the normalized growth rate $|\mathcal{M}_T|$ (a), (b) and the frequency shifts $\Delta\omega$ (c), (d) behave qualitatively the same in overdense plasma, e.g., $|\Omega_e|/\omega_p = 0.8$ (a), (c), and in underdense plasma, e.g., $|\Omega_e|/\omega_p = 1.2$ (b), (d). As α_2 increases from 0° to 180°, $|\mathcal{M}_T|$ increases monotonously for scattering from the upper resonance. For scattering off the lower resonance, $|\mathcal{M}_T|$ hits zero near $\alpha_2 \sim 176°$, where electron and ion contributions exactly cancel, and then increase to finite value at exact backscattering. In contrast, when the laser is scattered from the bottom resonance, $|\mathcal{M}_T|$ strongly peaks near $\alpha_2 \sim 170°$, and becomes zero for exact backward scattering. See text for how $|\mathcal{M}_T|$ scales with plasma parameters.

To see how $\mathcal{M}_T^b$ climbs up from zero, consider another special case where $\mathbf{k}_2$ is in the plane spanned by $\mathbf{k}_1$ and $\mathbf{b}$. In this case, it is more natural to consider $\mathcal{M}_T$ as function of α_2, the angle between $\mathbf{k}_1$ and $\mathbf{k}_2$, as plotted in Fig. 4. Let us find the asymptotic expression of $\mathcal{M}_T^b$ when $\alpha_2 \sim \pi$. In this limit, we have $\theta_3 \sim \pi/2$, and the resonance frequency ω_3 can be approximated by Eq. (B16). Then, the magnetization ratios $\beta_{3,e}^2 \simeq \Omega_e^2/\Omega_i^2 + |\Omega_e|/(\Omega_i \cos^2\theta_3)$ and $\beta_{3,i}^2 \simeq 1 + \Omega_i/(|\Omega_e|\cos^2\theta_3)$. Consequently, the magnetization factors can be well approximated by $\gamma_{3,e}^2 \simeq -1/\beta_{3,e}^2$ and $\gamma_{3,i}^2 \simeq -|\Omega_e|\cos^2\theta_3/\Omega_i$. Moreover, since $\omega_{1,2} \gg \omega_3$, the angle $\theta_3 \simeq \alpha_2/2$ and the wave vector $k_3 \simeq 2k_1 \sin(\alpha_2/2)$. Substituting these into Eq. (116), we see when $\alpha_2 \sim \pi$, the normalized growth rate

$$|\mathcal{M}_T^b|^2 \simeq \frac{\left[\zeta\left(1+\zeta\cos^2\frac{\alpha_2}{2}\right)\right]^{3/2}\sin^2\frac{\alpha_2}{2}\cos\frac{\alpha_2}{2}}{r^3 + r\left[1+\zeta\left(1+\zeta\cos^2\frac{\alpha_2}{2}\right)^2\right]\sin^2\frac{\alpha_2}{2}}, \quad (127)$$

where $r := |\Omega_e|/\omega_p$ and $\zeta := M_i/Z_i \gg 1$. To see the lowest order angular dependence, we can use a cruder but simpler approximation $|\mathcal{M}_T^b|^2 \simeq \zeta^{1/2}\cos(\alpha_2/2)/r$. We see $|\mathcal{M}_T^b|$ increases sharply from zero away from exact backscattering. Using result (123), we find in the other limit $\alpha_2 \sim 0$ the normalized growth rate

$$|\mathcal{M}_T^b| \simeq \frac{\sin^2\frac{\alpha_2}{2}}{r^{1/2}}\left(1 - \frac{1}{\zeta}\tan^2\frac{\alpha_2}{2}\right)^{-3/4}. \quad (128)$$

We see scattering from the bottom resonance can be strong when the plasma is weakly magnetized, as long as the scattering angle is away from exact forward or backward scattering.

In summary, the *TTL* scattering in magnetized plasma is mostly due to density beating Eq. (113), and the modification due to the magnetic field can be represented by the normalized growth rate $\mathcal{M}_T$. In magnetized plasmas, cyclotronlike resonances, in addition to the Langmuir-type resonance, contribute to the scattering of the T waves. When scattered from the Langmuir-type resonance, both the wave energy coefficient and the scattering strength are finite. Therefore, in this case, the angular dependence of $\mathcal{M}_T$ comes mostly from k_3, which reaches maximum for backscattering. In contrast, for scattering from cyclotronlike resonances, both the scattering strength and the wave energy coefficient can blow up. Their ratio $\mathcal{M}_T$ goes to zero when the scattering angles are such that the L wave frequency approaches either zero or the cyclotron frequencies. In addition, $\mathcal{M}_T$ can also become zero at special angles where scattering from electrons and ions exactly cancel. Away from these special angles, scattering from cyclotronlike resonances, which increase with decreasing magnetic field, typically have growth rates that are comparable to scattering from Langmuir-type resonances. When the plasma parameters are known, we can determine the angular dependence of $\mathcal{M}_T$ using Eq. (116). This knowledge can be used to choose injection angles of two lasers such that their scattering is either enhanced or suppressed. Conversely, by measuring angular dependence of $\mathcal{M}_T$ in laser scattering experiments, one may be able to fit plasma parameters to match Eq. (116). This provides a diagnostic method from which the magnetic field, as well as the plasma density and composition, can be measured.

B. $L \rightleftharpoons L + L$ scattering

In this section, we consider the other scenario where the three-wave scattering happens between three resonant quasilongitudinal waves. This happens, for example, when we launch an electrostatic wave into the plasma by some antenna arrays. When the wave power is strong enough to overcome damping, namely, when the damped growth rate [Eq. (85)] is positive, the pump wave may subsequently decay to two other waves that satisfy the resonance conditions. The decay waves are not necessarily electrostatic, but for the purpose of illustrating the general results in Sec. III, we will only give examples where the two decay waves are also electrostatic.

The coupling strength between three L waves can be simplified using the approximation that the waves are quasilongitudinal. Substituting $\mathbf{e}_i \simeq \hat{\mathbf{k}}_i$ into (79) and using the frequency resonance condition (62), the normalized scattering strength for *LLL* scattering can be written as

$$\begin{aligned}\Theta^s \simeq & -\frac{ck_1\omega_1}{\omega_2\omega_3}(\hat{\mathbf{k}}_1\cdot\mathbb{F}_{s,2}^*\hat{\mathbf{k}}_2)(\hat{\mathbf{k}}_1\cdot\mathbb{F}_{s,3}^*\hat{\mathbf{k}}_3)\\ & + \frac{ck_2\omega_2}{\omega_3\omega_1}(\hat{\mathbf{k}}_2\cdot\mathbb{F}_{s,1}\hat{\mathbf{k}}_1)(\hat{\mathbf{k}}_2\cdot\mathbb{F}_{s,3}^*\hat{\mathbf{k}}_3)\\ & + \frac{ck_3\omega_3}{\omega_1\omega_2}(\hat{\mathbf{k}}_3\cdot\mathbb{F}_{s,1}\hat{\mathbf{k}}_1)(\hat{\mathbf{k}}_3\cdot\mathbb{F}_{s,2}^*\hat{\mathbf{k}}_2), \quad (129)\end{aligned}$$

where $k_i := |\mathbf{k}_i|$ is the magnitude of the wave vector, and $\hat{\mathbf{k}}_i$ is the unit vector along $\mathbf{k}_i$ direction. It is easy to recognize that $\hat{\mathbf{k}}_i \cdot (\mathbb{F}_{s,j}/\omega_j)\hat{\mathbf{k}}_j$ is the projection of quiver velocity $\hat{\mathbf{v}}_j$ in $\hat{\mathbf{k}}_i$ direction. Therefore, the couplings between three L waves may also be interpreted as density beating. The first term in Θ^s is proportional to the rate of creating wave 1 by annihilating waves 2 and 3, the second term is proportional to the rate of annihilating waves 3 and $\bar{1}$ to create wave $\bar{2}$, and the last term can be interpreted similarly. The interference between these processes determines the overall scattering strength.

Having obtained expressions for the normalized scattering strength (129) and wave energy (112), we can immediately evaluate the coupling coefficient (83), and find expressions for experimental observables. For example, the linear growth rate γ_0 [Eq. (84)] of the parametric decay instability can be written as

$$\gamma_0 = \gamma_L |\mathcal{M}_L|, \tag{130}$$

where γ_L is purely determined by the pump wave

$$\gamma_L = \tfrac{1}{2} c k_1 |a_1|. \tag{131}$$

The normalized growth rate for *LLL* scattering

$$\mathcal{M}_L = \frac{\omega_p}{2ck_1}\left(\frac{\omega_p^2}{\omega_2\omega_3}\right)^{1/2}\mu_L \tag{132}$$

is the product of a kinematic factor with the coupling coefficient $\Gamma = \omega_p^2\mu/4$. In the *LLL* approximation, the normalized coupling coefficient

$$\mu_L \simeq \sum_s \frac{Z_s}{M_s}\frac{\omega_{ps}^2}{\omega_p^2}\frac{\Theta_r^s}{(u_1u_2u_3)^{1/2}}, \tag{133}$$

where Θ_r^s is the real part of Eq. (129). Again, notice when density of species s goes to zero, its contribution to μ_L also goes to zero as expected.

To evaluate the normalized growth rate $\mathcal{M}_L$, we can use the following procedure to mimic what happens in an actual experiment. Suppose we know the species density and magnetic field, then we know what resonances are there in the plasma. We can then launch a pump wave at resonance frequency ω_1 using some antenna array. The antenna array not only injects a wave at the given frequency, but also selects the wave vector k_1 and the wave direction θ_1. To observe the decay waves, we can place a probe at some angle θ_2 with respect to the magnetic field, and some azimuthal angle ϕ_2 in a spherical coordinate. The probe can measure fluctuations of the plasma potential and therefore inform us about the wave frequency ω_2. Then, we immediately know $\omega_3 = \omega_1 - \omega_2$ from the three-wave resonance condition. Moreover, since the third wave is a magnetic resonance, the frequency ω_3 constrains the angle θ_3 at which the third wave can propagate. However, a simple probe cannot measure the wave vector, so we will have to solve k_2 and k_3 from the resonance condition (61), which can be written in components as

$$k_3^2 = k_1^2 + k_2^2 - 2k_1k_2\cos\alpha_2, \tag{134}$$

$$k_3\cos\theta_3 = k_1\cos\theta_1 - k_2\cos\theta_2. \tag{135}$$

Here, $\alpha_2 = \alpha_2(\theta_1,\theta_2,\phi_2)$ is the angle between $\mathbf{k}_1$ and $\mathbf{k}_2$. The above system of quadratic equations has two solutions in general. This degeneracy comes from the symmetry $2 \leftrightarrow 3$ because we cannot distinguish whether the probe is measuring wave 2 or wave 3, both of which are electrostatic resonances. If the solutions k_2 and k_3 are both real and positive, the three-wave resonance conditions can be satisfied. Then, three-wave decay will happen once the pump amplitude a_1 exceeds the damping threshold, for which the damped growth rate [Eq. (85)] becomes positive. In other words, we control ω_1 and $\mathbf{k}_1$ by the antenna array, measure ω_2 using probes, and infer ω_3, $\mathbf{k}_2$, and $\mathbf{k}_3$ by solving resonance conditions. With this information, the analytical formula for the normalized growth rate $\mathcal{M}_L$ can be readily evaluated numerically.

1. *Parallel pump*

To demonstrate how to evaluate the normalized growth rate $\mathcal{M}_L$, consider the example where the pump wave is launched along the magnetic field ($\theta_1 = 0$). In an electron-ion plasma, this geometry allows the antenna to launch three electrostatic waves: the Langmuir wave, the electron cyclotron wave, or the ion cyclotron wave. In the regime where $\omega_p \sim |\Omega_e| \sim |\omega_p - \Omega_e| \gg \Omega_i$, four decay modes are allowed by the resonance conditions: $u \to l + l$, $l \to l + l$, $l \to l + b$, and $b \to b + b$, where we have labeled waves by the resonance branch they belong to, and u, l, and b denote the upper, lower, and bottom resonances.

First, let us consider the case where the pump wave is the Langmuir wave [Figs. 5(a) and 5(b)]. In this case, the magnetization factor γ_1 is finite, the wave energy coefficient $u_1 = 1$, and $\mathbb{F}_{s,1}\hat{\mathbf{k}}_1 = \hat{\mathbf{k}}_1$. The normalized scattering strength (129) contains the following four simple inner products: $(\hat{\mathbf{k}}_1 \cdot \mathbb{F}_{s,2}^*\hat{\mathbf{k}}_2) = (\hat{\mathbf{k}}_2 \cdot \mathbb{F}_{s,1}\hat{\mathbf{k}}_1) = \cos\theta_2$; $(\hat{\mathbf{k}}_1 \cdot \mathbb{F}_{s,3}^*\hat{\mathbf{k}}_3) = (\hat{\mathbf{k}}_3 \cdot \mathbb{F}_{s,1}\hat{\mathbf{k}}_1) = \cos\theta_3$, as well as two other inner products $(\hat{\mathbf{k}}_2 \cdot \mathbb{F}_{s,3}^*\hat{\mathbf{k}}_3) = \cos\theta_2\cos\theta_3 - \gamma_{s,3}^2\sin\theta_2\sin\theta_3$; and $(\hat{\mathbf{k}}_3 \cdot \mathbb{F}_{s,2}^*\hat{\mathbf{k}}_2) = \cos\theta_3\cos\theta_2 - \gamma_{s,2}^2\sin\theta_3\sin\theta_2$. Substituting these inner products into Eq. (129), and using the resonance condition (135), the normalized scattering strength can be immediately found. In the above expressions, θ_2 is the independent variable, and ω_2 is measured. Then, we can determine θ_3 from $\omega_3(\theta_3) = \omega_1 - \omega_2$ using Eq. (B10), and solve for k_2 and k_3 from Eqs. (134) and (135). Finally, with the above information, the normalized matrix element $\mathcal{M}_L$ can be readily evaluated.

When pumped at the Langmuir frequency ($\omega_1 = \omega_p$), the resonance conditions constrain the plasma parameters and angles at which the three-wave decay can happen. In overdense plasma [e.g., Fig. 5(a)], the Langmuir wave is in the upper resonance, so the resonance condition can be satisfied only if $\omega_p < 2|\Omega_e|$. Having satisfied this condition, the $u \to l + l$ decay can happen if $\theta_2 < \theta_b^o$, where θ_b^o is the angle such that $\omega_l(\theta_b^o) = \omega_p - |\Omega_e|$. In comparison, in underdense plasma [e.g., Fig. 5(b)], the Langmuir wave is in the lower resonance, and therefore can always decay. One decay mode is $l \to l + l$, which can happen for $\theta_2 > \theta_a^u$, where $\omega_l(\theta_a^u) = \omega_p - \omega_{LH}$. Another decay mode is $l \to l + b$. When $\omega_2 = \omega_l$, this decay mode happens for $0 < \theta_2 < \theta_i^u$, where $\omega_l(\theta_i^u) = \omega_p - \Omega_i$; whereas when $\omega_2 = \omega_b$, this decay mode can happen at any

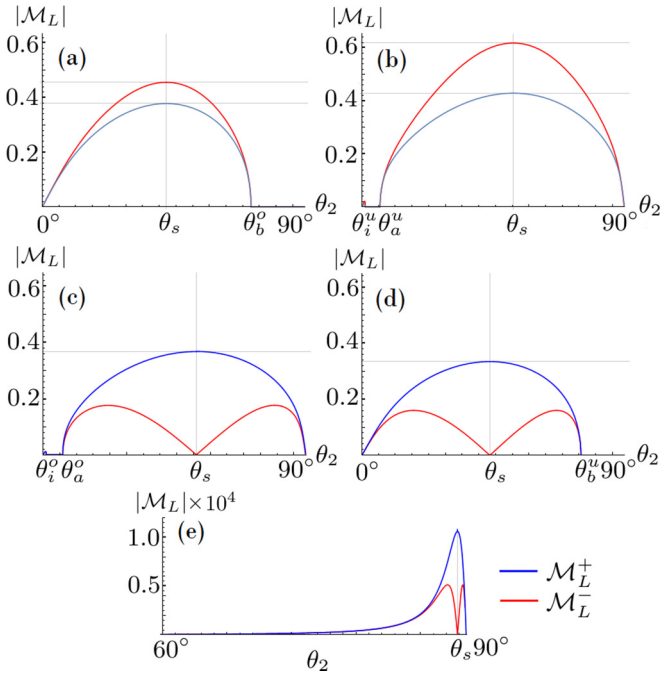

FIG. 5. Scattering of a parallel electrostatic pump wave in uniform hydrogen plasmas, when observed at angle θ_2 with respect to $\mathbf{k}_1 \parallel \mathbf{B}_0$. At each θ_2, due to the degeneracy $2 \leftrightarrow 3$, the wave vector has two possible values $k_2^{\pm}$, corresponding to $\mathcal{M}_L^+$ (blue, $\theta_3 > 90^\circ$) and $\mathcal{M}_L^-$ (red, $\theta_3 < 90^\circ$). The pump wave can be the Langmuir wave (a), (b); the electron cyclotron wave (c), (d); and the ion cyclotron wave (e). The normalized growth rate attains local extrema for symmetric scattering, where the two decay waves have the same frequency $\omega_r(\theta_s) = \omega_1/2$. In overdense plasma, e.g., $|\Omega_e|/\omega_p = 0.8$ (a), (c), $u \to l,l$ happens for $\theta_2 < \theta_b^o$, where $\omega_l(\theta_b^o) = \omega_p - |\Omega_e|$; $l \to l,l$ happens for $\theta_2 > \theta_a^o$, where $\omega_l(\theta_a^o) = |\Omega_e| - \omega_{LH}$; and $l \to l_2,b_3$ happens for $\theta_2 < \theta_i^o$, where $\omega_l(\theta_i^o) = |\Omega_e| - \Omega_i$. In underdense plasma, e.g., $|\Omega_e|/\omega_p = 1.2$ (b), (d), $u \to l,l$ happens for $\theta_2 < \theta_b^u$, where $\omega_l(\theta_b^u) = |\Omega_e| - \omega_p$; $l \to l,l$ happens for $\theta_2 > \theta_a^u$, where $\omega_l(\theta_a^u) = \omega_p - \omega_{LH}$; and $l \to l_2,b_3$ happens for $\theta_2 < \theta_i^u$, where $\omega_l(\theta_i^u) = \omega_p - \Omega_i$. Regardless of plasma density (e), $b \to b,b$ can always happen, for which the growth rate peaks near $\theta_s \sim 88^\circ$, where the decay is symmetrical. The gray lines indicate the symmetric angles and the asymptotic maxima obtained in the text.

θ_2. Finally, using the symmetry $2 \leftrightarrow 3$, the constraints on θ_3 can be readily deduced.

For Langmuir wave pump, the normalized growth rate reaches maximum for symmetric decay, where $\omega_2 = \omega_3 = \omega_p/2$. Let us find the asymptotic expression of $\mathcal{M}_L$ in the symmetric case, so as to get a sense of how the normalized growth rate scales with plasma parameters. The symmetric angle θ_s can be solved from Eq. (B10). Using $\omega_p \sim |\Omega_e| \gg \Omega_i$, we find $\sin^2\theta_s \simeq 3[1 - \omega_p^2/(4\Omega_e^2)]/4$. Then, the wave energy coefficient $u_2 = u_3 \simeq 1 + 3\omega_p^2/(4\Omega_e^2 - \omega_p^2)$, where the subdominant ion contribution in Eq. (112) has been dropped. To solve for the degenerate wave vectors in the symmetric case, it is more convenient to consider the two limits $\theta_2 = \theta_s - \phi, \theta_3 = \theta_s + \phi$, and $\theta_2 = \theta_s - \phi, \theta_3 = \pi - \theta_s - \phi$, and then let $\phi \to 0$. Solving Eqs. (134) and (135) for the wave vectors, the two solutions are $k_2^-/k_1 \simeq 1/(2\cos\theta_s)$ and $k_2^+/k_1 \simeq \sin\theta_s/(2\sin\phi)$. For the k_2^- solution, all terms are finite, and the normalized scattering strength is dominated by electron contribution $\Theta_e^- \simeq -3ck_1[1 + \omega_p^2/(2\Omega_e^2)]/(4\omega_p)$. Consequently, the normalized growth rate for symmetric k^- scattering

$$\mathcal{M}_L^-\left(\omega_p \to \frac{\omega_p}{2}, \frac{\omega_p}{2}\right) \simeq \frac{3}{4}\left(1 - \frac{\omega_p^2}{4\Omega_e^2}\right). \tag{136}$$

Notice that this decay mode can happen only if $|\Omega_e| \geqslant \omega_p/2$. To see what happens to the k_2^+ solution, we need to keep the dominant terms, and expand $\omega_2 \simeq \omega_p/2 - \omega_s'\phi$ and $\omega_3 \simeq \omega_p/2 + \omega_s'\phi$, where the angular derivative of lower resonance $\omega_l(\theta)$ can be evaluated at the symmetric angle using Eq. (B10) to be $\omega_s'/\omega_p \simeq -2\Omega_e^2\sin(2\theta_s)/(2\Omega_e^2 + \omega_p^2)$. Since ion terms do not contain singularity, the normalized scattering strength is again dominated by electrons $\Theta_e^+ \simeq 3ck_1[1 + 5\omega_p^2/(4\Omega_e^2)]/(8\omega_p)$. Consequently, the normalized growth rate for symmetric k^+ scattering is

$$\mathcal{M}_L^+\left(\omega_p \to \frac{\omega_p}{2}, \frac{\omega_p}{2}\right) \simeq -\frac{\mathcal{M}_L^-}{2}\left(1 + \frac{3\omega_p^2/2}{\omega_p^2 + 2\Omega_e^2}\right), \tag{137}$$

where $\mathcal{M}_L^-$ is given by Eq. (136). Since $\omega_p \leqslant 2|\Omega_e|$, it is easy to see that $|\mathcal{M}_L^+|$ is always smaller than $|\mathcal{M}_L^-|$. Moreover, wave damping tends to be smaller for the k_2^- solution. Therefore, the dominant decay mode in experiments will be the k^- mode, where the two decay waves propagate symmetrically at angle θ_s with respect to the parallel pump wave.

Second, let us consider the case where the pump wave is the electron cyclotron wave [Figs. 5(c) and 5(d)]. In this case, $\beta_{e,1} \sim 1$ and the magnetization factor $\gamma_{e,1}^2 \simeq (\Omega_e^2/\omega_p^2 - 1)/\sin^2\theta_1$ approaches infinity, so the dominant contribution comes from electrons. Keeping track of dominate terms as $\theta_1 \to 0$ and using small angle expansion (B11), the inner products $(\hat{\mathbf{k}}_2 \cdot \mathbb{F}_{e,1}\hat{\mathbf{k}}_1) \simeq \mp\gamma_{e,1}^2\sin\theta_1\sin\theta_2$ and $(\hat{\mathbf{k}}_3 \cdot \mathbb{F}_{e,1}\hat{\mathbf{k}}_1) \simeq \pm\gamma_{e,1}^2\sin\theta_1\sin\theta_3$. The other four inner products that enter Eq. (129) are the same as before. Keeping terms $\propto 1/\sin\theta_1$, the leading term of the normalized scattering strength can be readily found. Although the normalized scattering strength is divergent as $\theta_1 \to 0$, the normalized growth rate remains finite. This is because the divergence in Θ_e cancels the divergence in the wave energy coefficient $u_1 \simeq (\omega_p^2 - \Omega_e^2)^2/(\omega_p^2\Omega_e^2\sin^2\theta_1)$, which enters the denominator of $\mathcal{M}_L$. Following the procedure in the first example, the normalized growth rate can be readily obtained.

When intense electron cyclotron pump ($\omega_1 = |\Omega_e|$) exceeds the damping threshold, a number of decay modes are possible. In overdense plasma [e.g., Fig. 5(c)], the electron cyclotron wave is in the lower resonance, and three-wave decay is always possible. One decay mode is $l \to l + l$, which can happen for $\theta_2 > \theta_a^o$, where $\omega_l(\theta_a^o) = |\Omega_e| - \omega_{LH}$. Another decay mode is $l \to l + b$, which can happen for any θ_2 if $\omega_2 = \omega_b$, and can happen for $0 < \theta_2 < \theta_i^o$ if $\omega_2 = \omega_l$, where $\omega_l(\theta_i^o) = |\Omega_e| - \Omega_i$. In comparison, in underdense plasma [e.g., Fig. 5(d)], the electron cyclotron wave is in the upper resonance. The resonance condition can be satisfied if $|\Omega_e| < 2\omega_p$, and $u \to l + l$ decay can happen if $\theta_2 < \theta_b^u$, where $\omega_l(\theta_b^u) = |\Omega_e| - \omega_p$. We see the angular constraints for electron cyclotron pump decay are reciprocal to that of the Langmuir pump.

For electron cyclotron pump, the normalized growth rate crosses zero and therefore vanishes for symmetric k^- decay, while reaching maximum for symmetric k^+ decay. Let us find the asymptotic expression for $\mathcal{M}_L^+$ to get a sense of how the normalized growth rate scales with plasma parameters. Again, we can find the symmetric angle θ_s from Eq. (B10), which gives $\sin^2\theta_s \simeq 3[1-\Omega_e^2/(4\omega_p^2)]/4$. Then, the wave energy coefficients $u_2 = u_3 \simeq 2(1+2\omega_p^2/\Omega_e^2)/3$. To find the leading behavior of the scattering strength, consider the limit $\theta_2 = \theta_s - \phi, \theta_3 = \pi - \theta_s - \phi$, and let $\phi \to 0$. In this limit, the wave vector $k_2^+/k_1 \simeq \sin\theta_s/(2\sin\phi) \to \infty$, and the frequencies can be expanded by $\omega_2 \simeq \omega_p/2 - \omega_s'\phi$ and $\omega_3 \simeq \omega_p/2 + \omega_s'\phi$, where the angular derivative ω_s' can again be solved from Eq. (B10) to be $\omega_s'/\Omega_e \simeq 2\omega_p^2\sin(2\theta_s)/(\Omega_e^2 + 2\omega_p^2)$. Keeping the dominant terms as $\phi \to 0$, the normalized scattering strength $|\Theta_e^+| \simeq ck_1\sin(2\theta_s)(1-r^2)(1-r^2/4)/(\sin\theta_1\Omega_e)$, where $r := |\Omega_e|/\omega_p$. Since the ion contributions are subdominant, the normalized growth rate for symmetric $k+$ scattering is

$$\left|\mathcal{M}_L^+\left(\Omega_e \to \frac{\Omega_e}{2}, \frac{\Omega_e}{2}\right)\right| \simeq \frac{r}{4}\frac{\sqrt{(3-3r^2/4)^3(1+3r^2/4)}}{2+r^2}. \quad (138)$$

We see $\mathcal{M}_L^+$ is nonzero for $0 < r < 2$, and reaches a maximum of $\sim$0.38 when $r \sim 0.92$. The normalized growth rate can be related to the decay rate in experiments, once wave damping is taken into account.

Finally, let us consider the case where the electrostatic pump wave is at ion cyclotron frequency [Fig. 5(e)]. Since Ω_i is much smaller than any other characteristic wave frequencies, the only possible decay mode is $b \to b + b$. Such decay can happen for any angle θ_2 because the resonance conditions can always be satisfied. Similar to what happens in the previous example, the normalized growth rate $\mathcal{M}_L$ changes sign and therefore vanishes for symmetric k^- decay, while reaching maximum for symmetric k^+ decay. Now, let us give an estimate of the maximum value of $\mathcal{M}_L^+$. Since the magnetization factor $\gamma_{1,i}^2 \simeq \zeta/\tan^2\theta_1 \to \infty$, where $\zeta := M_i/Z_i \gg 1$, the ion terms dominate. The divergent inner products are $(\hat{\mathbf{k}}_2 \cdot \mathbb{F}_{i,1}\hat{\mathbf{k}}_1) \simeq \mp\gamma_{i,1}^2\sin\theta_1\sin\theta_2$ and $(\hat{\mathbf{k}}_3 \cdot \mathbb{F}_{i,1}\hat{\mathbf{k}}_1) \simeq \pm\gamma_{i,1}^2\sin\theta_1\sin\theta_3$. The other four inner products are finite and similar to what we have before. Using these inner products and keeping the leading terms, the normalized scattering $|\Theta_i^+| \simeq ck_1\Omega_e^2\cos\theta_s/(2\Omega_i^3\sin\theta_1)$, where we have expanded near the symmetric angle as before, with $\omega_s' \simeq 9\Omega_e\sin(2\theta_s)/16$. The symmetric angle, very close to $\pi/2$, can be estimated from Eq. (B16) to be $\cos^2\theta_s \simeq \Omega_i/(3|\Omega_e|)$. The wave energy coefficients $u_1 \simeq \omega_p^2|\Omega_e|/(\Omega_i^3\sin^2\theta_1)$ and $u_2 = u_3 \simeq 16\omega_p^2/(9\Omega_i|\Omega_e|)$. Substituting these results into formula (133), the normalized growth rate for symmetric k^+ decay is

$$\left|\mathcal{M}_L^+\left(\Omega_i \to \frac{\Omega_i}{2}, \frac{\Omega_i}{2}\right)\right| \simeq \frac{3\sqrt{3}}{32}\frac{\Omega_i}{\omega_p}. \quad (139)$$

We see in a typical plasma where $\omega_p \gg \Omega_i$, the decay mode $b \to b + b$ is orders of magnitude weaker than the other decay modes. Nevertheless, when compared with the pump frequency $\omega_1 = \Omega_i$, the growth rate of the three-wave decay instability is not necessarily small.

2. *Perpendicular pump*

In this section, we use another set of examples to illustrate how to evaluate the normalized growth rate $\mathcal{M}_L$, by considering the cases where the pump wave propagates perpendicular to the magnetic field. In this geometry, the pump frequency can either be the upper-hybrid frequency ω_{UH} or the lower-hybrid frequency ω_{LH}, in an electron-ion plasma. For three-wave decay to happen, the frequency resonance condition (62) must be satisfied. Since the lower-hybrid frequency $\omega_{LH} \gg \Omega_i$, it is not possible to match the frequency resonance condition with a *LH* pump wave in a uniform plasma. By similar consideration, for a *UH* pump wave, the decay mode $u \to u + u$ is also forbidden. However, other decays modes of the *UH* pump are possible. Using expression $\omega_{UH}^2 \simeq \omega_p^2 + \Omega_e^2$, we see that $u \to u + b$ is always possible; $u \to u + l$ is possible if $2/\sqrt{\zeta} \lesssim r \lesssim \sqrt{\zeta}/2$, where $\zeta = M_i/Z_i \gg 1$ is the normalized charge-to-mass ratio for ions; and $u \to l + l$ is possible only if $1/\sqrt{3} \leqslant r \leqslant \sqrt{3}$. Here, $r = |\Omega_e|/\omega_p$ is the ratio of electron cyclotron frequency to the plasma frequency. In this section, we will consider r in the range where all three decay modes are possible.

In addition to the frequency condition, the wave vector resonance conditions (61) must also be satisfied for three-wave decay to happen. To see when Eq. (61) can be satisfied in this perpendicular geometry, it is convenient to discuss in the spherical coordinate where the polar angle θ is measured from the magnetic field $\mathbf{b}$, and the azimuthal angle ϕ is measured from $\mathbf{k}_1$. In this spherical coordinate, the wave vectors $\mathbf{k}_2$ and $\mathbf{k}_3$ are constrained on the two cones spanning angles $\theta_2, \pi - \theta_2$ and $\theta_3, \pi - \theta_3$. Then, $\mathbf{k}_2$ and $\mathbf{k}_3$ can reside along the lines generated by cutting the two cones with a plane passing through $\mathbf{k}_1$. When $|\cos\theta_2| > |\cos\theta_3|$, the plane starts to intercept both cones when $|\cos\phi_3| \geqslant |\cos\phi_c|$, where the critical angle $\sin\phi_c = \tan\theta_2/\tan\theta_3$. When the strict inequality holds, for each $\mathbf{k}_3$, there are two solutions to $\mathbf{k}_2$ such that the resonance condition (61) is satisfied. By the exchange symmetry $2 \leftrightarrow 3$, we immediately know what happens when $|\cos\theta_2| < |\cos\theta_3|$. The resonance condition (61) constrains where in the $\theta_2 - \phi_2$ plane the normalized growth rate $\mathcal{M}_L$ take nonzero values.

Having matched the resonance conditions, the normalized growth rate in the polar coordinate can be readily evaluated (Fig. 6). To understand the angular dependence of $\mathcal{M}_L$, it is useful to notice that due to the exchange symmetry $\mathcal{M}_L(2,3) = \mathcal{M}_L(3,2)$, the normalized growth rate $\mathcal{M}_L(\theta_2,\phi_2)$ in one region can be mapped to $\mathcal{M}_L(\theta_2',\phi_2')$ in anther region. To be more specific, when ω_2 is on the upper resonance [Fig. 6(a)], the normalized growth rate $\mathcal{M}_L$ is nonzero in two regions. The first region is $\theta_2 < \theta_u^a$, where $\omega_u(\theta_u^a) = \omega_{UH} - \omega_{LH}$. In this region, the decay mode $u_1 \to u_2 + l_3$ is allowed, where ω_3 is on the lower resonance. By the exchange symmetry, this region can be mapped to the island on the bottom right corner of Fig. 6(b), in which ω_2 is on the lower resonance instead. The other region in Fig. 6(a) where $\mathcal{M}_L$ is nonzero is the narrow strip $\theta_2 > \theta_u^b$, where $\omega_u(\theta_u^b) = \omega_{UH} - \Omega_i$. In this region, the decay mode $u_1 \to u_2 + b_3$ is allowed, where ω_3 is on the bottom resonance. Exchanging $2 \leftrightarrow 3$, this region corresponds to the case where ω_2 is on the bottom resonance instead [Fig. 6(c)]. The remaining decay mode is $u_1 \to l_2 + l_3$, where both decay waves are on the lower resonance. This decay mode is allowed

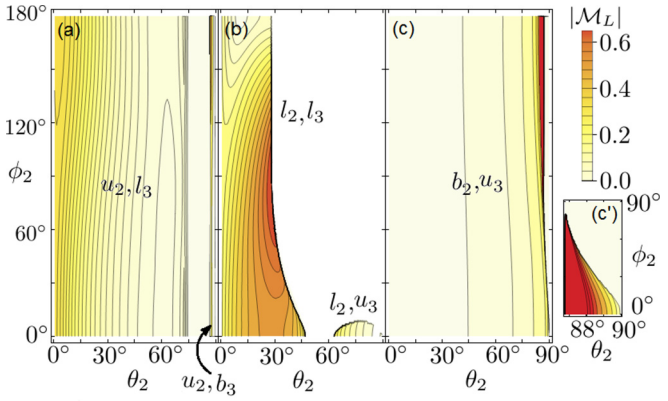

FIG. 6. Normalized growth rate $|\mathcal{M}_L|$ when pumped by an upper-hybrid wave ($\mathbf{k}_1 \perp \mathbf{B}_0$) in a uniform hydrogen plasma with $|\Omega_e|/\omega_p = 1.2$. The growth rates are observed at polar angle θ_2 with respect to $\mathbf{B}_0$ and azimuthal angle ϕ_2 with respect to $\mathbf{k}_1$. When ω_2 is on the upper resonance (a), the $u \to u_2,l_3$ decay can happen for $\theta_2 < \theta_u^a$, where $\omega_u(\theta_u^a) = \omega_{UH} - \omega_{LH}$. In this case, an important decay channel has $\omega_2 \sim |\Omega_e|$ propagating almost parallel to $\mathbf{B}_0$ in the backward direction, and $\omega_3 \gg \omega_{LH}$ propagating almost perpendicular to $\mathbf{B}_0$ in the forward direction. This region corresponds to the l_2,u_3 region in (b), in which ω_2 is on the lower resonance instead. The other decay mode is $u \to u_2,b_3$, which can happen in the narrow strip $\theta_2 > \theta_u^b$ in (a), where $\omega_u(\theta_u^b) = \omega_{UH} - \Omega_i$. Equivalently, exchanging the labels to b_2,u_3, this decay mode can happen in the colored region in (c), in which ω_2 is on the bottom resonance instead. For this decay mode, the dominant decay channel has $\omega_2 \sim \omega_{UH}$ propagating almost perpendicular to $\mathbf{B}_0$ in the forward direction, and $\omega_3 \sim \Omega_i$ propagating either in the forward or backward direction. The last decay mode is $u \to l_2,l_3$, which corresponds to the large colored region in (b). For this decay mode, the dominant decay channel is the symmetric decay, where $\omega_2 \sim \omega_3 \sim \omega_{UH}/2$ and both waves propagate at angles with $\mathbf{B}_0$ in the forward direction.

within the large region on the left of Fig. 6(b). This region has a straight boundary at $\theta_2 = \theta_l^m$, where $\omega_l(\theta_l^m) = \omega_{UH}/2$. To the left of this boundary, we have $\theta_2 < \theta_3$, so there is only one solution for k_2. To the right of this boundary, we have $\theta_2 > \theta_3$, so both k_2^- and k_2^+ solutions exist as long as $\sin\phi_2 < \tan\theta_3/\tan\theta_2$. Whenever both solutions exist, Fig. 6 shows the k^- branch, which has weaker damping. In those degenerate cases, the k^+ branch is usually comparable with the k^- branch. An exception is inserted in Fig. 6(c′), where the k^+ branch is dominant for $u_1 \to b_2 + u_3$ decay, corresponding to the forward scattering of the *UH* pump with little frequency shift.

For the $u \to u_2 + l_3$ decay [Fig. 6(a)], one important decay channel has $\omega_2 \sim |\Omega_e|$ propagating almost parallel to $\mathbf{b}$ in the backward direction ($\phi_2 = 180^\circ$), and the other decay wave propagating almost perpendicular to $\mathbf{b}$ in the forward direction ($\phi_3 = 0^\circ$). To see how $\mathcal{M}_L$ scales with plasma parameters, let us find its asymptotic expression when $\theta_2 \to 0$. In this limit $\omega_2 \to |\Omega_e|$, so the magnetization factor $\gamma_{2,e}^2$ is divergent. Then, the dominant terms of the coupling strength (129) come from the $\mathbb{F}_{e,2}$ terms. The divergent inner products are $(\hat{\mathbf{k}}_1 \cdot \mathbb{F}_{e,2}^* \hat{\mathbf{k}}_2) \simeq -\gamma_{e,2}^2 \sin\theta_2$ and $(\hat{\mathbf{k}}_3 \cdot \mathbb{F}_{e,2}^* \hat{\mathbf{k}}_2) \simeq -\gamma_{e,2}^2 \sin\theta_2 \sin\theta_3$, and we also need the finite inner products $(\hat{\mathbf{k}}_1 \cdot \mathbb{F}_{e,3}^* \hat{\mathbf{k}}_3) \simeq \gamma_{e,3}^2 \sin\theta_3$ and $(\hat{\mathbf{k}}_3 \cdot \mathbb{F}_{e,1} \hat{\mathbf{k}}_1) \simeq \gamma_{e,1}^2 \sin\theta_3$. Then, the leading term of the normalized scattering strength is $\Theta_e \simeq ck_1\gamma_{e,1}^2\gamma_{e,2}^2\gamma_{e,3}^2(\omega_1^2 - \omega_3^2)\sin\theta_2 \sin\theta_3/(\omega_1\omega_2\omega_3)$, where we have used the resonance condition $k_3 \sin\theta_3 = k_1$. The angle θ_3 can be estimated from Eq. (B10) using $\omega_3 \gg \Omega_i$, which gives $\sin^2\theta_3 \simeq (\omega_3^2 - \omega_p^2)(\omega_3^2 - \Omega_e^2)/(\omega_p^2\Omega_e^2)$. Then, the wave energy coefficient $u_3 \simeq (2\omega_3^2 - \omega_{UH}^2)(\omega_3^2 - \Omega_e^2)$. As for the other two wave energy coefficients, using previous results, we know $u_1 = \omega_{UH}^2/\omega_p^2$ and $u_2 \simeq (\Omega_e^2 - \omega_p^2)^2/(\Omega_e^2\omega_p^2\sin^2\theta_2)$. Substituting these into Eqs. (132) and (133), we find the normalized growth rate

$$|\mathcal{M}_L(\omega_{UH} \to |\Omega_e|,\omega_3)| \simeq \frac{\omega_3(\omega_3 + \omega_{UH})}{\omega_p\sqrt{2(\omega_{UH}^2 - 2\omega_3^2)}}, \qquad (140)$$

where $\omega_3 = \omega_{UH} - |\Omega_e|$ is the resonance frequency. From previous discussion, we know this decay mode can happen as long as $1/\sqrt{3} \leqslant r \lesssim \sqrt{\zeta}/2$. Within this parameter range, it is easy to see that Eq. (140) decreases monotonically with increasing magnetic field. The maximum value $\mathcal{M}_L = \sqrt{3}/2$ is attained at $r = 1/\sqrt{3}$, where $\omega_3 = |\Omega_e| = \omega_{UH}/2$ such that the decay is symmetric.

For the $u \to l_2 + l_3$ decay [Fig. 6(b)], the dominant decay channel is the symmetric decay, where $\omega_2 = \omega_3 = \omega_1/2$. In the symmetric decay geometry, we have $\theta_3 = \pi - \theta_2$ and $\phi_3 = -\phi_2$. Then, the wave vector resonance condition becomes $k_2 = k_3 = k_1/(2\sin\theta_2\cos\phi_2)$. The symmetric decay angle $\theta_2 = \theta_s$ can be estimated from Eq. (B10) using $\omega_2 = \omega_{UH}/2 \gg \Omega_i$, which gives $\cos^2\theta_s \simeq 3\omega_{UH}^4/(16\omega_p^2\Omega_e^2)$. Since the frequencies are far away from cyclotron frequencies, all the magnetization factors are finite. Then, the inner products $(\hat{\mathbf{k}}_1 \cdot \mathbb{F}_{s,2}^* \hat{\mathbf{k}}_2) \simeq \gamma_{s,2}^2(\cos\phi_2 + i\beta_{s,2}\sin\phi_2)\sin\theta_2$, $(\hat{\mathbf{k}}_2 \cdot \mathbb{F}_{s,1} \hat{\mathbf{k}}_1) \simeq \gamma_{s,1}^2(\cos\phi_2 + i\beta_{s,1}\sin\phi_2)\sin\theta_2$, $(\hat{\mathbf{k}}_3 \cdot \mathbb{F}_{s,2}^* \hat{\mathbf{k}}_2) \simeq -1 + \gamma_{s,2}^2\sin^2\theta_2(2\cos^2\phi_2 + i\beta_{s,2}\sin 2\phi_2 - \beta_{s,2}^2)$, and by exchanging $2 \leftrightarrow 3$, we can easily find the other three inner products. Substituting these inner products into Eq. (129), the normalized scattering strength becomes particularly simple when $\phi_2 \to \pi/2$. In this limit $k_2,k_3 \to \infty$, but the product $k_2\cos\phi_2 = -k_3\cos\phi_3$ remains finite. Keeping nonzero terms as $\phi_2 \to \pi/2$, the scattering strength simplifies to $\Theta_e^+ \simeq -2ck_1\omega_{UH}^3/[\omega_p^2(3\Omega_e^2 - \omega_p^2)]$. The electron terms also dominate the wave energy coefficients $u_2 = u_3 \simeq 2\omega_{UH}^2/(3\Omega_e^2 - \omega_p^2)$. Gathering the above results, the normalized growth rate for symmetric k^+ scattering is

$$\left|\mathcal{M}_L^+\left(\omega_{UH} \to \frac{\omega_{UH}}{2},\frac{\omega_{UH}}{2}\right)\right| \simeq \frac{\omega_p}{\omega_{UH}}. \qquad (141)$$

The above special value of $\mathcal{M}_L$ is approximately the maximum in Fig. 6(b), where $\theta_2 = \theta_s$ and $\phi_2 = 90^\circ$. Notice that this special case is singular in wave vector $k_2,k_3 \to \infty$, and hence will be suppressed by wave damping. Therefore, the dominant decay channels observed in experiment will happen at smaller angle $\phi_2 < 90^\circ$ in the symmetric decay geometry.

Finally, for the $u \to b_2 + u_3$ decay [Fig. 6(c)], the dominant decay channel has $\omega_2 \sim \omega_{UH}$ propagating almost perpendicular to $\mathbf{b}$ in the forward direction, and $\omega_3 \sim \Omega_i$ propagating either in the forward or backward direction. As an example, let us consider symmetric forward scattering where $\phi_2 = \phi_3 = 0$ and $\theta_2 = \pi - \theta_3 = \theta_s$. In this geometry, $k_2^- = k_3^- = k_1/(2\sin\theta_s)$. Since $\theta_s \sim \pi/2$, we can estimate the symmetric angle using asymptotic expressions Eqs. (B14) and (B16).

Substituting these expressions into the frequency resonance condition (62), we obtain $\cos^2\theta_s \simeq 2\Omega_i\omega_{UH}^3/(\Omega_e^2\omega_p^2) \sim 0$, where we have used that $\omega_p^2|\Omega_e|/(2\omega_{UH}^3) \lesssim 0.2$ is always a small number. Then, the wave energy $u_2 \simeq u_1 = \omega_{UH}^2/\omega_p^2$ and $u_3 \simeq \omega_p^2[1+2\omega_{UH}^3/(\omega_p^2|\Omega_e|)]^2/(\Omega_i|\Omega_e|)$. Now that the magnetization factors are all finite, the inner products are simply $(\hat{\mathbf{k}}_1\cdot\mathbb{F}_{s,2}^*\hat{\mathbf{k}}_2) \simeq \gamma_{s,2}^2\sin\theta_2$, $(\hat{\mathbf{k}}_2\cdot\mathbb{F}_{s,1}\hat{\mathbf{k}}_1) \simeq \gamma_{s,1}^2\sin\theta_2$, $(\hat{\mathbf{k}}_3\cdot\mathbb{F}_{s,2}^*\hat{\mathbf{k}}_2) \simeq \cos\theta_3\cos\theta_2 + \gamma_{2,s}^2\sin\theta_3\sin\theta_2$, and the three other inner products can be obtained by exchanging $2\leftrightarrow 3$. Again, the scattering is mostly due to electrons, for which $\gamma_{e,1}^2 \simeq \gamma_{e,2}^2 \simeq \omega_{UH}^2/\omega_p^2$ and $\gamma_{e,3}^2 \simeq -\omega_3^2/\Omega_e^2 \ll \cos\theta_s^2$. Therefore, the dominant term comes from the second line of Eq. (129), which gives the scattering strength $\Theta_e^- \simeq -ck_1\Omega_i\omega_{UH}^5/(\omega_3\Omega_e^2\omega_p^4)$. Substituting these results into (132) and (133), we immediately see that the normalized growth rate for forward scattering is

$$|\mathcal{M}_L^-(\omega_{UH}\to\omega_{UH},\Omega_i)| \simeq \frac{\omega_p}{4\sqrt{\omega_{UH}|\Omega_e|}}\left(\frac{\omega_3}{\Omega_i}\right)^{1/2}, \quad (142)$$

where $\omega_3 = \omega_b(\theta_s) \sim \Omega_i$ can be obtained from Eq. (B16). Using the above result, we can also find the symmetric nearly backward scattering $\mathcal{M}_L^+$ by replacing the coefficient $\frac{1}{4}$ with $k_2^+/(2k_1)$. The symmetric nearly backward scattering channel has divergent k_2^+, and therefore can have very large growth rate in the absence damping.

VI. CONCLUSION AND DISCUSSION

In summary, we solve the cold fluid-Maxwell system to second order in the multiscale perturbation series in the most general geometry (Sec. II), where waves in a discrete spectrum interact in triplets through quadratic nonlinearities [Eq. (51)]. Due to $\mathbf{v}_{s1}\times\mathbf{B}_1$, $\mathbf{v}_{s1}\cdot\nabla_{(0)}\mathbf{v}_{s1}$, and $\nabla_{(0)}\cdot(n_{s1}\mathbf{v}_{s1})$ nonlinearities, three-wave scatterings change the envelopes of "on-shell" waves as they advect, as well as generate a spectrum of "off-shell" quasimodes due to wave beating. By introducing the forcing operator [Eq. (26)], we manage to give a convenient formula [Eq. (53)] for the scattering strength $\mathbf{S}_{\mathbf{q},\mathbf{q}'}$ in the most general geometry.

When there are only three resonant "on-shell" waves participating in the interaction (Sec. III), the scattering strengths [Eq. (71)] are closely related due to action conservation. The action conservation laws are manifested by the three-wave equations [Eqs. (80)–(82)], which describe how the amplitudes of waves evolve, regardless of the changes in their phases and polarizations. The three-wave equations contain one essential parameter, the coupling coefficient [Eq. (83)], whose explicit formula is given in terms of the wave energy coefficient [Eq. (75)] and the normalized scattering strength [Eq. (78)]. The coupling coefficient contains five degrees of freedom, and can be readily evaluated once the participating waves and their geometry are specified.

The general formula for the scattering strength becomes particularly transparent once we quantize the classical three-wave Lagrangian. Using the quantized Lagrangian [Eq. (102)], all six terms of the scattering strength arise from a single cubic interaction $\propto P^i(\partial_i A_j)J^j$ as six permutations of the Feynman diagrams [Eq. (105)]. We postulate that this form of the three-wave interaction is independent of the plasma model that one uses to calculate the linear response. In this paper, the linear response is calculated using the cold fluid model. More generally, the linear response may be calculated using the kinetic model or even quantum models. Then, using the relation between the S matrix element and the three-wave scattering strength [Eq. (106)], the three-wave coupling coefficient may be directly computed without going through the perturbative solution of the equations.

To demonstrate how to evaluate the cold fluid coupling coefficient, we give a set of examples where all three participating waves are either quasitransverse (T) or quasilongitudinal (L) (Sec. V). As an experimental observable, we compute the growth rate of the three-wave decay instability [Eq. (84)], which is proportional to the coupling coefficient when wave damping is ignored. For *TTL* decay (Sec. V A), the scattering is due to density perturbation of the L wave, and the normalized growth rate is given conveniently by Eqs. (116) and (117). For *LLL* decay (Sec. V B), the scattering is due to density beating of three L waves, and the normalized growth rate is given by the explicit Eqs. (129), (132), and (133). We evaluate these equations numerically for the cases where the pump wave is either parallel or perpendicular to the magnetic field, while the decay waves propagate at arbitrary angles. To facilitate understanding of the angular dependencies, we also find asymptotic expressions of the normalized growth rate in limiting cases.

The above examples elucidate the previously unknown angular dependence of three-wave scattering when strong magnetic field is present. In contrast to the unmagnetized case, backscattering is not necessarily the fastest growing instability in a magnetized plasma. For example, in the *TTL* scattering (Figs. 2–4), which happens when two lasers interact via a magnetic resonance, exact backscattering may be suppressed, while nearly perpendicular scattering may be enhanced. For another example, in the *LLL* scattering (Figs. 5 and 6), which can happen when an electrostatic wave launched by antenna arrays decays to two other longitudinal waves, symmetric decays are usually favored whenever possible, but asymmetric decays can also be important at special angles.

The above collisionless, cold, fluid results will need to be modified when kinetic or collisional effects become important. Aside from wave damping [Eq. (85)], a major modification comes from the alternation of the linear eigenmode structure, which will be constituted of Bernstein waves instead of the hybrid waves. In addition, weak coupling results obtained in this paper will need to be modified when three-wave interactions become strong. This happens when wave amplitudes become nonperturbative, so that relativistic effects become non-negligible, and linear eigenmode structure becomes strongly distorted.

Despite the above caveats, the importance of this work is twofold. First, the formulation we have developed preserves the general mathematical structure, thereby enabling profound simplifications of the most general results. From these results, illuminating physical consequences are extracted, which can be used to develop reduced models and benchmark numerical simulations. Second, the uniform, collisionless, and cold

fluid results we have obtained serve as the baseline for understanding angular dependence of three-wave scattering in magnetized plasmas, which is important for magnetic confinement devices, as well as laser-plasma interactions in magnetized environment.

ACKNOWLEDGMENTS

We would like to thank the anonymous referees for their comments and suggestions. This research is supported by NNSA Grant No. DE-NA0002948 and DOE Research Grant No. DE-AC02-09CH11466.

APPENDIX A: MULTISCALE PERTURBATIVE SOLUTION OF SYSTEM OF ODES

In Sec. II, we use a multiscale expansion to solve a system of nonlinear hyperbolic partial differential equations. To facilitate understanding of the multiscale expansion, here we demonstrate how it can be successfully applied to the following system of ordinary differential equations, which are hyperbolic in the absence of perturbations

$$\dot{x} = y + \epsilon f(x,y), \tag{A1}$$

$$\dot{y} = -x + \epsilon g(x,y). \tag{A2}$$

Here, $\dot{x}$ and $\dot{y}$ denote the time derivatives of $x(t)$ and $y(t)$, respectively, f and g are some polynomials, and $\epsilon \ll 1$ is a small parameter.

The above system of equations may be solved perturbatively using the expansion

$$x(t) = x_0(t) + \epsilon x_1(t) + \epsilon^2 x_2(t) + \cdots, \tag{A3}$$

$$y(t) = y_0(t) + \epsilon y_1(t) + \epsilon^2 y_2(t) + \cdots. \tag{A4}$$

However, naive perturbative solutions using only the above expansions will fail due to nonlinearity, by which the notorious secular terms will arise. The secular terms grow monotonically in time and will quickly render the perturbative solutions invalid. To remove the secular terms, it is necessary that we also expand the time scales

$$t = t_0 + \frac{1}{\epsilon} t_1 + \frac{1}{\epsilon^2} t_2 + \cdots, \tag{A5}$$

$$\partial_t = \partial_0 + \epsilon \partial_1 + \epsilon^2 \partial_2 + \cdots, \tag{A6}$$

where one unit of the slow time scale t_n worth $1/\epsilon^n$ units of the fastest time scale t_0. Different time scales can be regarded as independent, and the total time derivative can be written as the summation of derivatives on each time scale $\partial_n := \partial/\partial t_n$. Substituting expansions (A3)–(A6) into Eqs. (A1) and (A2) and collect terms according to their order in ϵ, we can obtain a series of equations.

The ϵ^0-order equations are simply the equations for a simple harmonic oscillator

$$\partial_0 x_0 - y_0 = 0, \tag{A7}$$

$$\partial_0 y_0 + x_0 = 0. \tag{A8}$$

For real valued x and y, the general solution is well known:

$$x_0 = a_0 e^{it_0} + \text{c.c.}, \tag{A9}$$

$$y_0 = i a_0 e^{it_0} + \text{c.c.}, \tag{A10}$$

where c.c. stands for complex conjugate, and the complex amplitude $a_0 = a_0(t_1, t_2, \ldots)$ can be a function of slow variables. If we truncate the solution on this order, then x and y oscillate harmonically with constant amplitude. On the other hand, if we move on to the next order, perturbations $\epsilon f(x,y)$ and $\epsilon g(x,y)$ will cause the amplitude a_0 to vary on slow time scales, as will be described by higher order equations.

The ϵ^1-order equations start to couple perturbations on different time scales

$$\partial_1 x_0 + \partial_0 x_1 - y_1 - f_0 = 0, \tag{A11}$$

$$\partial_1 y_0 + \partial_0 y_1 + x_1 - g_0 = 0, \tag{A12}$$

where $f_0 = f(x_0, y_0)$ and $g_0 = g(x_0, y_0)$, in which x_0 and y_0 are given by Eqs. (A9) and (A10). The above two equations contain three unknowns x_1, y_1, and $\partial_1 a_0$. Therefore, we can use the extra degree of freedom to remove secular terms. To do that, let us first separate variables x_1 and y_1 and rewrite the ϵ^1-order equations as

$$\partial_0^2 x_1 + x_1 + 2\partial_1 y_0 = u_1, \tag{A13}$$

$$\partial_0^2 y_1 + y_1 - 2\partial_1 x_0 = v_1, \tag{A14}$$

where the source terms

$$u_1[a_0] = \partial_0 f_0 + g_0, \tag{A15}$$

$$v_1[a_0] = \partial_0 g_0 - f_0. \tag{A16}$$

Substituting x_0 and y_0 into polynomials f and g, we can write $f_0 = \sum_n f_{0n} e^{int_0} + \text{c.c.}$, and $g_0 = \sum_n g_{0n} e^{int_0} + \text{c.c.}$, where f_{0n} and g_{0n} are some functionals of a_0. Then, the source terms can be written similarly as $u_1 = \sum_n u_{1n} e^{int_0} + \text{c.c.}$ and $v_1 = \sum_n v_{1n} e^{int_0} + \text{c.c.}$, where $u_{1n} = g_{0n} + i n f_{0n}$ and $v_{1n} = -f_{0n} + i n g_{0n}$.

To solve the ϵ^1-order equations (A13) and (A14), we can match coefficients of Fourier exponents and split the equations into two sets. The first set of equations govern how the amplitude a_0 evolves on the slow time scale t_1, which can be written as $\partial_1 x_0 = -\frac{1}{2}(v_{11} e^{it_0} + \text{c.c.})$ and $\partial_1 y_0 = \frac{1}{2}(u_{11} e^{it_0} + \text{c.c.})$. These two equations are essentially the same, as can be seen from the relations between x_0 and y_0, as well as the definitions of u_{11} and v_{11}. Both of these equations result in the same equation for a_0, which absorbs the secular term

$$\partial_1 a_0 = \tfrac{1}{2}(f_{01} - i g_{01}), \tag{A17}$$

where the right-hand side is some functional of a_0. This first order ordinary differential equation (ODE) of a_0 can usually be integrated, from which a_0 will be a known function of t_1. The other sets of equations govern x_1 and y_1:

$$\partial_0^2 x_1 + x_1 = \sum_{n \neq 1} u_{1n} e^{\text{int}} + \text{c.c.}, \tag{A18}$$

$$\partial_0^2 y_1 + y_1 = \sum_{n \neq 1} v_{1n} e^{\text{int}} + \text{c.c.} \tag{A19}$$

Having removed the secular terms, the above equations are now secular free, and can be readily solved by

$$x_1 = a_1 e^{it_0} + \sum_{n\neq 1} \frac{u_{1n}}{1-n^2} e^{\text{int}_0} + \text{c.c.}, \tag{A20}$$

$$y_1 = b_1 e^{it_0} + \sum_{n\neq 1} \frac{v_{1n}}{1-n^2} e^{\text{int}_0} + \text{c.c.} \tag{A21}$$

The amplitudes a_1 and b_1 are clearly related by the ϵ^1-order equations, which give

$$b_1 = ia_1 - \tfrac{1}{2}(f_{01} + ig_{01}). \tag{A22}$$

Notice that in the perturbation series (A3), we can always redefine $a_0 + \epsilon a_1 \to a_0'$. Hence, it is sufficient to set the amplitude $a_1 = 0$. In this way, we will obtain a x-majored solution, where the amplitude of e^{it_0} for x is completely given by a_0, whereas amplitude e^{it_0} for y is given by the summation $b_0 + \epsilon b_1 + \cdots$. Alternatively, by setting $b_1 = 0$, we can obtain a y-majored solution, which we will not pursue here. For three-wave scattering studied in this paper, it is sufficient to truncate the solution series at this order.

To show the general structure of the multiscale expansion, here, it is instructive to carry out the solution to the next order. The ϵ^2-order equations are

$$\partial_2 x_0 + \partial_1 x_1 + \partial_0 x_2 - y_2 - f_1 = 0, \tag{A23}$$

$$\partial_2 y_0 + \partial_1 y_1 + \partial_0 y_2 + x_2 - g_1 = 0, \tag{A24}$$

where $f_1 = x_1\partial_x f_0 + y_1\partial_y f_0$ and $g_1 = x_1\partial_x g_0 + y_1\partial_y g_0$. In the above two equations, there are three unknowns x_2, y_2, and $\partial_2 a_0$. So, again, we can use the extra degree of freedom to remove the secular terms. Separating variables x_2 and y_2, we can rewrite the equations as

$$\partial_0^2 x_2 + x_2 + 2\partial_2 y_0 = u_2, \tag{A25}$$

$$\partial_0^2 y_2 + y_2 - 2\partial_2 x_0 = v_2. \tag{A26}$$

Since we set $a_1 = 0$ for the x-majored solution, the source terms are functionals of a_0 only:

$$u_2[a_0] = \partial_0 f_1 + g_1 + \partial_1^2 x_0 - 2\partial_1 y_1 - \partial_1 f_0, \tag{A27}$$

$$v_2[a_0] = \partial_0 g_1 - f_1 + \partial_1^2 y_0 + 2\partial_1 x_1 - \partial_1 g_0. \tag{A28}$$

Since f and g are polynomials, we can write $f_1 = \sum_n f_{1n} e^{\text{int}_0} + \text{c.c.}$ and $g_1 = \sum_n g_{1n} e^{\text{int}_0} + \text{c.c.}$ Then, the source terms can be written similarly as $u_2 = \sum_n u_{2n} e^{\text{int}_0} + \text{c.c.}$ and $v_2 = \sum_n v_{2n} e^{\text{int}_0} + \text{c.c.}$, where $v_{21} = iu_{21} = i\partial_1^2 a_0 + ig_{11} - \partial_1 g_{01} - f_{11}$, and for $n \geqslant 2$, we have $u_{2n} = inf_{1n} - \partial_1 f_{0n} + g_{1n} - 2\partial_1 v_{1n}/(1-n^2)$ and $v_{2n} = ing_{1n} - \partial_1 g_{0n} + f_{1n} + 2\partial_1 u_{1n}/(1-n^2)$.

To solve the ϵ^2-order equations (A25) and (A26), we can use a similar procedure to split the equations into two sets. The first set of equations can be written as a single equation governing how the amplitude a_0 evolve on the slow time scale t_2:

$$\partial_2 a_0 = \frac{1}{2}(f_{11} - ig_{11}) - \frac{i}{4}\partial_1(f_{01} + ig_{01}). \tag{A29}$$

Regarding t_1 as a parameter, the above equation is a first order ODE for $a_0(t_2)$, which can usually be integrated. The second set of equations is similar to Eqs. (A18) and (A19), with u_{1n} and v_{1n} replaced by u_{2n} and v_{2n}, respectively. The solutions to these secular-free equations are similar to Eqs. (A20) and (A21) with the order index "1" replaced by the order index "2" in which the second order amplitudes a_2 and b_2 are related by the ϵ^2-order equations

$$b_2 = ia_2 - \frac{1}{2}(f_{11} + ig_{11}) - \frac{i}{4}\partial_1(f_{01} + ig_{01}). \tag{A30}$$

To obtain the x-majored solution, we again set a_2 to zero. By the obvious analogy between the ϵ^1- and ϵ^2-order equations, the above procedures can be readily extended to higher order in the perturbation series.

To see how the multiscale expansion works in practice, interested readers are encouraged to try the following two examples. The first is a linear example, where $f(x,y) = -x$ and $g(x,y) = 0$. In this case, the exact solution can be easily obtained. The second is a nonlinear example, where $f(x,y) = 0$ and $g(x,y) = -x + 2x^3$. The exact solutions to this nonlinear example are the Jacobi elliptic functions. One can expand the exact solutions in ϵ, and check order by order that they match the perturbative solution obtained using the multiscale expansion.

APPENDIX B: LINEAR WAVES IN COLD MAGNETIZED PLASMAS

In Sec. II A, we obtain the first order electric field equation (33) in the momentum space. The solutions to this matrix equation give the linear eigenmodes of the cold fluid-Maxwell system. In this appendix, we review properties of the linear waves, in order to facilitate understanding of their scatterings discussed in this paper.

To discuss properties of the linear waves, it is convenient to choose the coordinate system where the uniform magnetic field is in the z direction. In this coordinate, the forcing operator (26) has matrix representation

$$\mathbb{F}_{s,\mathbf{k}} = \begin{pmatrix} \gamma_{s,\mathbf{k}}^2 & i\beta_{s,\mathbf{k}}\gamma_{s,\mathbf{k}}^2 & 0 \\ -i\beta_{s,\mathbf{k}}\gamma_{s,\mathbf{k}}^2 & \gamma_{s,\mathbf{k}}^2 & 0 \\ 0 & 0 & 1 \end{pmatrix}. \tag{B1}$$

Having fixed the z axis, we can rotate the coordinate system, such that the wave vector $\mathbf{k} = (k_\perp, 0, k_\parallel) = k(\sin\theta, 0, \cos\theta)$, where θ is the angle between $\mathbf{k}$ and $\mathbf{b}$. In this coordinate system, the matrix representation of the dispersion tensor (34) can be easily found. Then, the first order electric field equation $\mathbb{D}_{\mathbf{k}}\mathcal{E}_{\mathbf{k}}^{(1)}/\omega_{\mathbf{k}}^2 = 0$ can be written as

$$\begin{pmatrix} S - n_\parallel^2 & -iD & n_\perp n_\parallel \\ iD & S - n^2 & 0 \\ n_\perp n_\parallel & 0 & P - n_\perp^2 \end{pmatrix} \begin{pmatrix} \mathcal{E}_x^{(1)} \\ \mathcal{E}_y^{(1)} \\ \mathcal{E}_z^{(1)} \end{pmatrix} = 0, \tag{B2}$$

where $n = ck/\omega$ is the refractive index, $n_\perp = n\sin\theta$, and $n_\parallel = n\cos\theta$ are projections in the perpendicular and parallel

directions. Following Stix's notations [36], the components of the dielectric tensor are

$$S = 1 - \sum_s \frac{\omega_{ps}^2}{\omega^2 - \Omega_s^2}, \tag{B3}$$

$$D = \sum_s \frac{\Omega_s}{\omega} \frac{\omega_{ps}^2}{\omega^2 - \Omega_s^2}, \tag{B4}$$

$$P = 1 - \sum_s \frac{\omega_{ps}^2}{\omega^2}. \tag{B5}$$

In the above expressions, we have omitted the $\mathbf{k}$ subscripts for both ω and $\mathcal{E}^{(1)}$. The expressions for S and D can be simplified, using identities in quasineutral electron-ion plasma, in which $n_e = Z_i n_i$, so $\Omega_i \omega_{pe}^2 + \Omega_e \omega_{pi}^2 = 0$ and $\Omega_i^2 \omega_{pe}^2 + \Omega_e^2 \omega_{pi}^2 + \omega_p^2 \Omega_e \Omega_i = 0$, where $\omega_p^2 = \sum_s \omega_{ps}^2$ is the plasma frequency squared.

The electric field equation (B2) has nontrivial solution if and only if the dispersion tensor is degenerate. This is equivalent to requiring the determinant of the dispersion tensor to be zero, which gives a constraint between ω and $\mathbf{k}$, called the dispersion relation. In the above coordinate system, using Stix's notation, the dispersion relation can be written as

$$An^4 - Bn^2 + C = 0, \tag{B6}$$

where the coefficients of the quadratic equation of n^2 are

$$A = S \sin^2\theta + P \cos^2\theta, \tag{B7}$$

$$B = RL \sin^2\theta + PS(1 + \cos^2\theta), \tag{B8}$$

$$C = PRL, \tag{B9}$$

which are functions of ω only, independent of the wave vector. In the above expressions, $R = S + D$ and $L = S - D$ are the right- and left-handed components of the dielectric tensor. The quadratic dispersion relation (B6) has two solutions $n_\pm^2 = (B \pm F)/(2A)$, where $F^2 = B^2 - 4AC = (RL - PS)^2 \sin^4\theta + 4P^2D^2\cos^2\theta$. Since $F^2 \geqslant 0$, we see the two solutions $n_\pm^2$ are both real. However, $n_\pm^2$ is not always positive, so each solution may contain many branches, emanating from cutoff frequencies ω_c, at which $C(\omega_c) = 0$ so that $n^2 = 0$. For example, in electron-ion plasma [Fig. 7(a)], the cutoff frequencies are at ω_R, ω_p, and ω_L, and the dispersion relation contains two electromagneticlike branches, for which $\omega \to ck$ as $k \to \infty$, as well as three electrostaticlike branches, for which $\omega \to \omega_r$ as $k \to \infty$, where ω_r is some resonance frequencies.

The resonance frequencies are asymptotic values of ω on electrostatic branches when $k \to \infty$. As the frequency approaches the resonance frequencies from below, the refractive index $n_\pm^2 \to \infty$, so we can find ω_r by solving $A(\omega_r) = 0$. In electron-ion plasma, this equation for resonance frequencies can be explicitly written as

$$0 = \omega_r^6 - \omega_r^4\left(\omega_p^2 + \Omega_e^2 + \Omega_i^2\right) - \omega_p^2\Omega_e^2\Omega_i^2\cos^2\theta + \omega_r^2\left[\omega_p^2\left(\Omega_e^2 + \Omega_i^2\right)\cos^2\theta - \omega_p^2\Omega_e\Omega_i\sin^2\theta + \Omega_e^2\Omega_i^2\right]. \tag{B10}$$

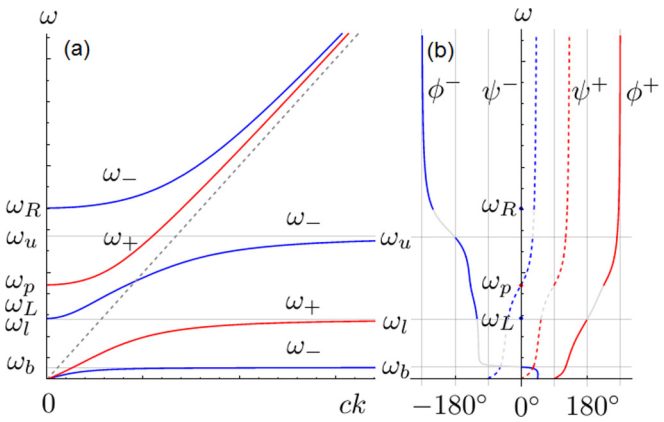

FIG. 7. Linear wave dispersion relations (a) and polarization angles (b) in a cold electron-ion plasma with $m_i/m_e = 10$ and $|\Omega_e|/\omega_{pe} = 1.2$, when $\theta = 45°$. Both the n_+^2 (red) and the n_-^2 (blue) solutions contain an electromagneticlike branch and electrostaticlike branches. The electromagneticlike branches asymptote to vacuum light wave $\omega \to ck$ when $k \to \infty$, where the waves become transverse ($\phi \to 90°$, mod 180°). The electrostaticlike branches asymptote to resonances $\omega \to \omega_r$ as $k \to \infty$, where the waves become longitudinal ($\phi \to 0°$, mod 180°). The waves are in general elliptically polarized ($\psi \neq 0°$, mod 90°), except at special angles.

The above cubic equation for ω_r^2 has three solutions (Fig. 8), which can be ordered from large to small as the upper (ω_u), lower (ω_l), and bottom (ω_b) resonance. When $\theta \sim 0$ or π, the resonance frequencies approach ω_p, $|\Omega_e|$, and Ω_i. Keeping the next order angular dependence, the three resonance frequencies, when $\sin\theta \sim 0$, can be approximated

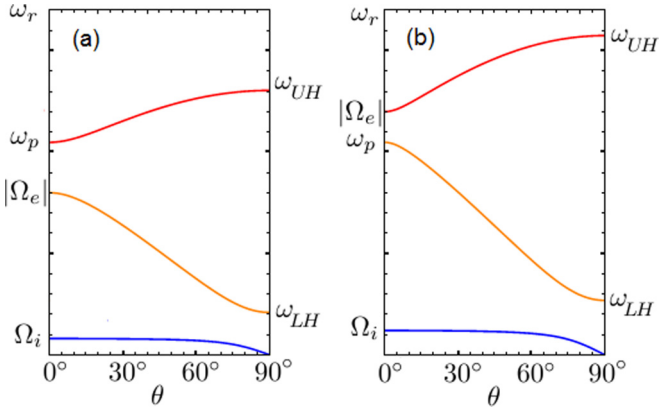

FIG. 8. Resonance frequencies in electron-ion plasma with $m_i/m_e = 10$. In overdense plasma, e.g., $|\Omega_e|/\omega_p = 0.8$ (a), as θ increases from 0° to 90°, the upper resonance (red) increases from ω_p to ω_{UH}; the lower resonance (orange) decreases from $|\Omega_e|$ to ω_{LH}; and the bottom resonance (blue) decreases from Ω_i to zero. In underdense plasma, e.g., $|\Omega_e|/\omega_p = 1.2$ (b), as θ increases from 0° to 90°, the upper resonance (red) increases from $|\Omega_e|$ to ω_{UH}; the lower resonance (orange) decreases from ω_p to ω_{LH}; and the bottom resonance (blue) decreases from Ω_i to zero. This figure can be used to read out the frequency shift $\Delta\omega$, once the scattering angle of the longitudinal wave is known.

by

$$\frac{\omega_r^2}{\omega_p^2} \simeq 1 - \frac{\Omega_e^2 \sin^2\theta}{\Omega_e^2(2-\cos^2\theta) - \omega_p^2}, \tag{B11}$$

$$\frac{\omega_r^2}{\Omega_e^2} \simeq 1 - \frac{\omega_p^2 \sin^2\theta}{\omega_p^2(2-\cos^2\theta) - \Omega_e^2}, \tag{B12}$$

$$\frac{\omega_r^2}{\Omega_i^2} \simeq 1 - \frac{\Omega_i}{|\Omega_e|}\tan^2\theta. \tag{B13}$$

In the other limit, when $\theta \sim \pi/2$, the resonance frequencies approach the upper-hybrid frequency ω_{UH}, the lower-hybrid frequency ω_{LH}, and 0. Keeping the next order angular dependence, the upper, lower, and bottom resonance frequencies, when $\cos\theta \sim 0$, can be approximated by

$$\frac{\omega_u^2}{\omega_{UH}^2} \simeq 1 - \frac{\omega_p^2\Omega_e^2\cos^2\theta}{\left(\omega_p^2+\Omega_e^2\right)^2 + \omega_p^2\Omega_e^2\cos^2\theta}, \tag{B14}$$

$$\frac{\omega_l^2}{\omega_{LH}^2} \simeq 1 + \frac{\Omega_e^2\cos^2\theta}{\Omega_e^2\cos^2\theta + |\Omega_e|\Omega_i(1+\cos^2\theta)}, \tag{B15}$$

$$\frac{\omega_b^2}{\Omega_i^2} \simeq \frac{|\Omega_e|\cos^2\theta}{\Omega_i + |\Omega_e|\cos^2\theta}. \tag{B16}$$

The above asymptotic expressions for resonance frequency ω_r are extremely useful when we approximate the scattering strength and wave energy coefficients.

When frequencies approach resonances, the waves become longitudinal. On the other hand, the wave becomes transverse when frequencies approach infinity. For intermediate frequencies, we can find the wave polarization by solving for eigenmodes of the electric field equation (B2). In the wave coordinate $\hat{\mathbf{k}}$,$\hat{\mathbf{y}}$, and $\hat{\mathbf{k}}\times\hat{\mathbf{y}}$, we can write $\mathcal{E}_k = \mathcal{E}\cos\phi$, $\mathcal{E}_y = -i\mathcal{E}\sin\phi\cos\psi$, and $\mathcal{E}_\times = \mathcal{E}\sin\phi\sin\psi$, where we have omitted the superscript of $\mathcal{E}^{(1)}$. Then, the polarization angles

$$\tan\psi = \frac{Sn^2 - RL}{n^2 D\cos\theta}, \tag{B17}$$

$$\tan\phi = \frac{P\cos\theta}{(n^2-P)\sin\theta\sin\psi}. \tag{B18}$$

Notice that $\mathcal{E}_\times/\mathcal{E}_y = i\tan\psi$ is imaginary. Therefore, the wave is elliptically polarized in general. Also notice that the polarization ray $\hat{\mathcal{E}}$ is invariant under transformations $(\phi,\psi) \to (\phi \pm 180^\circ, \psi)$ and $(\phi,\psi) \to (-\phi, \psi \pm 180^\circ)$. Therefore, the polarization angles [Fig. 7(b)] can be interpreted up to these identity transformations. Finally, notice that $\psi_\pm$ for the $n_\pm^2$ solutions satisfies the identity $\tan\psi_+\tan\psi_- = -1$. Hence, polarizations of these two frequency-degenerate eigenmodes are always orthogonal in the transverse plane.

[1] R. P. H. Chang and M. Porkolab, Phys. Rev. Lett. **32**, 1227 (1974).
[2] C. S. Liu and V. Tripathi, Phys. Rep. **130**, 143 (1986).
[3] N. J. Fisch, Phys. Rev. Lett. **41**, 873 (1978).
[4] N. J. Fisch, Rev. Mod. Phys. **59**, 175 (1987).
[5] M. Porkolab, Phys. Fluids **20**, 2058 (1977).
[6] R. Cesario, A. Cardinali, C. Castaldo, F. Paoletti, W. Fundamenski, S. Hacquin *et al.*, Nucl. Fusion **46**, 462 (2006).
[7] J. Myatt, H. Vu, D. DuBois, D. Russell, J. Zhang, R. Short, and A. Maximov, Phys. Plasmas **20**, 052705 (2013).
[8] M. Hohenberger, P.-Y. Chang, G. Fiksel, J. Knauer, R. Betti, F. Marshall, D. Meyerhofer, F. Séguin, and R. Petrasso, Phys. Plasmas **19**, 056306 (2012).
[9] S. A. Slutz and R. A. Vesey, Phys. Rev. Lett. **108**, 025003 (2012).
[10] O. V. Gotchev, P. Y. Chang, J. P. Knauer, D. D. Meyerhofer, O. Polomarov, J. Frenje, C. K. Li, M. J.-E. Manuel, R. D. Petrasso, J. R. Rygg *et al.*, Phys. Rev. Lett. **103**, 215004 (2009).
[11] Y. Shi, H. Qin, and N. J. Fisch, Phys. Rev. E **95**, 023211 (2017).
[12] R. Davidson, *Methods in Nonlinear Plasma Theory* (Elsevier, Amsterdam, 1972).
[13] J. Weiland and H. Wilhelmsson, *Coherent Non-linear Interaction of Waves in Plasmas*, International Series in Natural Philosophy (Pergamon, Oxford, 1977).
[14] U. Wagner, M. Tatarakis, A. Gopal, F. Beg, E. Clark, A. Dangor, R. Evans, M. Haines, S. Mangles, P. Norreys *et al.*, Phys. Rev. E **70**, 026401 (2004).
[15] J. Santos, M. Bailly-Grandvaux, L. Giuffrida, P. Forestier-Colleoni, S. Fujioka, Z. Zhang, P. Korneev, R. Bouillaud, S. Dorard, D. Batani *et al.*, New J. Phys. **17**, 083051 (2015).
[16] S. Fujioka, Z. Zhang, K. Ishihara, K. Shigemori, Y. Hironaka, T. Johzaki, A. Sunahara, N. Yamamoto, H. Nakashima, T. Watanabe *et al.*, Sci. Rep. **3**, 1170 (2013).
[17] A. Sjölund and L. Stenflo, Z. Phys. A **204**, 211 (1967).
[18] B. K. Shivamoggi, Phys. Scr. **25**, 637 (1982).
[19] C. Grebogi and C. Liu, Phys. Fluids **23**, 1330 (1980).
[20] H. C. Barr, T. J. M. Boyd, L. R. T. Gardner, and R. Rankin, Phys. Fluids **27**, 2730 (1984).
[21] A. Vyas, R. K. Singh, and R. Sharma, Phys. Plasmas **23**, 012107 (2016).
[22] H. Sanuki and G. Schmidt, J. Phys. Soc. Jpn. **42**, 664 (1977).
[23] N. M. Laham, A. S. A. Nasser, and A. M. Khateeb, Phys. Scr. **57**, 253 (1998).
[24] P. M. Platzman, P. A. Wolff, and N. Tzoar, Phys. Rev. **174**, 489 (1968).
[25] S. Ram, Phys. Plasmas **24**, 885 (1982).
[26] T. J. M. Boyd and R. Rankin, J. Plasma Phys. **33**, 303 (1985).
[27] L. Stenflo, J. Plasma Phys. **4**, 585 (1970).
[28] L. Stenflo, Phys. Scr. **T50**, 15 (1994).
[29] G. Brodin and L. Stenflo, Phys. Scr. **85**, 035504 (2012).
[30] J. Larsson, L. Stenflo, and R. Tegeback, J. Plasma Phys. **16**, 37 (1976).
[31] L. Stenflo, Phys. Scr. **T107**, 262 (2004).
[32] J. Galloway and H. Kim, J. Plasma Phys. **6**, 53 (1971).
[33] T. Boyd and J. Turner, J. Math. Phys. **19**, 1403 (1978).
[34] I. Y. Dodin and A. V. Arefiev, Phys. Plasmas **24**, 032119 (2017).
[35] L. Debnath, *Nonlinear Partial Differential Equations for Scientists and Engineers* (Springer, New York, 2011).

[36] T. Stix, *Waves in Plasmas* (AIP Press, New York, 1992).
[37] A. Jurkus and P. Robson, Proc. IEE-Part B: Electron. Commun. Eng. **107**, 119 (1960).
[38] J. Armstrong, N. Bloembergen, J. Ducuing, and P. Pershan, Phys. Rev. **127**, 1918 (1962).
[39] R. Harvey and G. Schmidt, Phys. Fluids **18**, 1395 (1975).
[40] J. Armstrong, S. Jha, and N. Shiren, IEEE J. Quantum Electron. **6**, 123 (1970).
[41] K. Nozaki and T. Taniuti, J. Phys. Soc. Jpn. **34**, 796 (1973).
[42] Y. Ohsawa and K. Nozaki, J. Phys. Soc. Jpn. **36**, 591 (1974).
[43] V. E. Zakharov and S. V. Manakov, Zh. Eksp. Teor. Fiz. **69**, 1654 (1975) [Sov. Phys. JETP **42**, 842 (1975)].
[44] J. G. Turner and M. Baldwin, Phys. Scr. **37**, 549 (1988).
[45] M. J. Ablowitz, D. J. Kaup, and A. C. Newell, Stud. Appl. Math. **53**, 249 (1974).
[46] D. J. Kaup, A. Reiman, and A. Bers, Rev. Mod. Phys. **51**, 275 (1979).
[47] Y. Shi, N. J. Fisch, and H. Qin, Phys. Rev. A **94**, 012124 (2016).